Numerical Studies of Shear-Induced Chaos

Erin Stafford, Katherine Johnston, and Obinna Ukogu

June 9, 2021

1 Introduction

In their 2008 paper on shear-induced chaos, Lin and Young investigate the use of shear in the production of chaos through a series of numerical studies [3]. In these studies, a sudden external force (a "kick") is repeatedly applied to a system with a stable limit cycle and is shown to produce chaotic behavior if applied strategically. Specifically, if points away from the limit cycle undergo non-uniform angular displacement (shear), the phase space may be folded as it relaxes towards the limit cycle in between kicks. This then may lead to positive Lyapunov exponents, an indicator of chaos.

This work follows a series of papers by Wang and Young that investigated this phenomenon analytically in the limiting case of infrequent forcing [4, 6, 5]. The primary contribution of this work was to numerically investigate examples that were intractable with current analytic methods. The numerical studies apply discrete kicks at periodic or random intervals, or continuous-time stochastic forcing to an oscillating system.

This project will focus on two cases of discrete kicks applied to systems with a stable limit cycle. In the first case, the system is kicked periodically with short-to-medium relaxation times between kicks, and in the second case, the second system is kicked with random amplitude at random times. The authors showed that in both systems, *shear-induced chaos* occurs when the shearing and the amplitude of the forcing are large enough to overcome the effects of the damping.

In what follows, we give a brief presentation (with added details) of the mechanism behind this phenomenon, describe the numerical setup and results from simulations, explore further the effect of randomness in producing chaos, and investigate shear-induced chaos in a predator-prey model.

2 Summary of Analytic Results

Consider a smooth flow ϕ_t on $M \subset \mathbb{R}^n$ and let γ be a hyperbolic limit cycle of the flow. This means that the eigenvalues of the linearized system, for directions transverse to γ, have negative real parts. Moreover, it is known that hyperbolic limit cycles are robust to small perturbations.

We apply kicks periodically to points on or near γ. A kick is essentially a mapping between points in M, denoted by $\kappa(x) : M \to M$. Assuming the kicks are applied every T time units, the evolution of the kicked system can be found by iterating the map $F_T(x) = \phi_T(\kappa(x))$, i.e. discretizing the flow. If the time between kicks (T) is large, since γ is an attractor there may exist a neighborhood $\mathcal{U}$ near and including γ such that kicked points in this neighborhood return to $\mathcal{U}$ between kicks, i.e. $F_T(\mathcal{U}) \subset \mathcal{U}$.

If this is the case, we define the attractor of the system $\Gamma = \Gamma(\kappa, T) = \cap_{n \geq 0} F_T^n(\mathcal{U})$ as the invariant set corresponding the periodically kicked limit cycle. Due to the robustness of hyperbolic limit cycle, for small kicks Γ may be a slightly deformed periodic orbit. However, stronger kicks may "break" the limit cycle leading to a more complicated invariant set like a strange attractor. Meanwhile, a (chaotic) strange attractor of a system is an attracting set (with fractal geometry) in which points that start close together move arbitrarily far apart over time (and vice versa). Strange attractors are generally indicators of chaos. The next theorem makes these ideas precise.

Theorem 1 ***(Creation of strange attractors from limit cycles)*** *Let ϕ_t be a C^4 flow with a hyperbo lic limit cycle γ . Then there is an open set of kick maps K with the following properties: for each $\kappa \in K$, there is a set $\Delta = \Delta(\kappa) \subset \mathbb{R}^+$ with Leb(Δ)> 0 such that for each $T \in \Delta$, Γ is a strange attractor of F_T.*

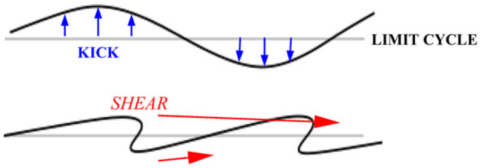

(a)

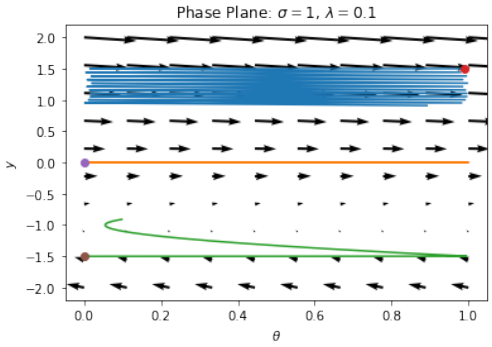

(b)

Figure 1: The stretch-and-fold action of a kick followed by relaxation in the presence of shear. (a) A cartoon showing the effect of shear [3]. (b) Phase plane for the unkicked system given in Theorem 2.

This theorem guarantees that, subject to some very mild requirements, we can always kick and relax a

system with a hyperbolic limit cycle so as to produce a strange attractor. However, it leaves open the possibility (as we will see) that the system may alternate between having a hyperbolic limit cycle and and a strange attractor as the parameters governing the kick are varied continuously. This phenomenon is known as *transient chaos* and has been extensively studied in the literature [2]. The proof of this theorem is rather technical so the reader is referred to [5] for details.

The rest of this paper is devoted to the investigation of how chaos can arise in this way for systems that undergo *shear*. Shear is a non-uniform twisting (translocation) of points that are not on the limit cycle, that is, the angular velocity of points away from the limit cycle depends on their position (Figure 1).

Theorem 2 *Consider the system*

$$\begin{aligned} \dot{\theta} &= 1 + \sigma y \\ \dot{y} &= -\lambda y + A \cdot H(\theta) \cdot \sum_{n=0}^{\infty} \delta(t - nT), \end{aligned} \tag{1}$$

where $(\theta, y) \in S^1 \times \mathbb{R}$ *are coordinates in the phase space,* $\lambda, \sigma, A > 0$ *are constants, and* $H : S^1 \to \mathbb{R}$ *is a nonconstant smooth function. If the quantity*

$$\frac{\sigma}{\lambda} \cdot A \equiv \frac{\textit{shear}}{\textit{contraction rate}} \cdot \textit{kick 'amplitude'}$$

is sufficiently large, then there is a positive measure set $\Delta \subset \mathbb{R}^+$ *such that for all* $T \in \Delta$, F_T *has a strange attractor.*

The reader is referred to [5] for a proof or this theorem. As stated, the kick is determined by $H(\theta)$ scaled by amplitude A. For the unkicked system ($A = 0$), the limit cycle is $\gamma = S^1 \times \{0\}$ and we can compute the Jacobian (J), eigenvalues (μ_1 and μ_2), and stable and center subspaces (E^s and E^c) of this system

$$J = \begin{bmatrix} 0 & \sigma \\ 0 & -\lambda \end{bmatrix} \Longrightarrow \mu_{1,2} = 0, -\lambda \Longrightarrow E^s = \text{span}\{(1, -\frac{\lambda}{\sigma})^T\},\ E^c = \text{span}\{(1,0)^T\}.$$

Since the system is linear, the local stable manifold through each point $\theta_0 \in \gamma$ equals the center subspace

$$W^s_{loc}(\theta_0, 0) = E^s(\theta_0, 0) = \{(\theta, y) | y = -\frac{\lambda}{\sigma}(\theta - \theta_0)\}). \tag{2}$$

This leads to the observation that the entire state space is foliated by local stable manifolds emanating from points on γ (Figure 2). We note, as can be seen from Equation 1, that points on γ rotate around the fixed point once per unit time, as do the stable manifolds.

With this in mind, we can think of kicking the system as pushing points onto new stable manifolds, along which they slide and shear as they relax down to possible new points on the limit cycle. Thus the limit cycle γ is repeatedly stretched and folding onto itself, which can form a strange attractor. Crucially, when $T >> 1$ i.e. kicks are infrequent, we can determine the unique point, $(\theta^*, 0)$, where a point initially at $(\theta, 0) \in \gamma$ will map to, at time $n + a$ with $a \in [0, 1)$ and $n \in \mathbb{Z}_+$, after being kicked.

We denote this family of maps, called the *singular limits* of the map F_T as $T \to \infty$, by

$$f_a(\theta) := \lim_{n\to\infty} \phi_{n+a}(\kappa(\theta)) \tag{3}$$

with parameter a, and where we have used the fact that the period of our system is 1 time unit. The computation for f_0 is as follows

$$\begin{aligned} A \cdot H(\theta) = y = -\frac{\lambda}{\sigma}(\theta\theta^*) \Longrightarrow f_0(\theta) = \theta^* = \theta + \frac{\lambda}{\sigma} A \cdot H(\theta) \\ \Rightarrow f_a(\theta) = \theta + a + \frac{\lambda}{\sigma} A \cdot H(\theta) \pmod 1 \end{aligned} \tag{4}$$

where we have used the fact that $f_a(\theta) = f_0(\theta) + a \pmod 1$ since points on γ travel with unit angular velocity. The behavior of this family of maps determines the attractor of the kicked system. When f_a is injective, the attractor Γ of the system will remain a hyperbolic fixed point, and when f_a fails to be injective that strange attractors may form. For more details, the reader is referred to [4, 6, 5].

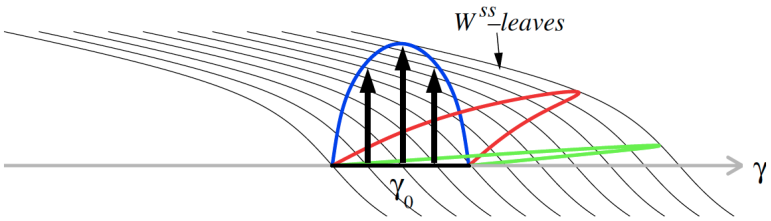

Figure 2: Each point on the limit cycle has a stable manifold that passes through it. The kicked limit cycle is stretched and folded as it slides along the stable manifolds [3].

3 Selected Reproduced Results

In between kicks the system defined in Theorem 2 can be solved exactly since

$$\begin{aligned} \dot{y} = -\lambda y \Longrightarrow y(t) = y_0 e^{-\lambda t}, \\ \dot{\theta} = 1 + \sigma y_0 e^{-\lambda t} \end{aligned}$$

which can be solved by integrating to yield

$$\theta(t) = \theta_0 + t + \frac{\sigma}{\lambda} y_0 (1 - e^{\lambda t}).$$

At $t = 0$, the system (θ_0, y_0) receives a kick, then evolves according to the relations above before being kicked again at time T. This simplifies the dynamics of the system which is reduced to a map:

$$\begin{aligned} \theta_T &= \theta_0 + T + \frac{\sigma}{\lambda} \left(y_0 + A \sin(2\pi\theta_0)\right) \cdot (1 - e^{-\lambda T}) \pmod 1, \\ y_T &= e^{-\lambda T}(y_0 + A \sin(2\pi\theta_0)). \end{aligned} \tag{5}$$

We call this the *map reduction* of the system. The Jacobian of the map is given by

$$J(\theta, y, T) = \begin{bmatrix} 1 + \frac{2\pi\sigma}{\lambda} A \cos(2\pi\theta)(1 - e^{-\lambda T}) & \frac{\sigma}{\lambda}(1 - e^{-\lambda T}) \\ e^{-\lambda T} 2\pi A \cos(2\pi\theta) & e^{-\lambda T} \end{bmatrix}.$$

Using this map reduction, we only need to iterate through the sequence of kick times to compute the dynamics of the system. Our goal is to compute the Lyapunov exponent of individual trajectories. In general, an 2-D system will have two Lyapunov exponents. Using the Jacobian of the map reduction we can compute Lyapunov exponents of a trajectory by tracking the effect of the Jacobian on an arbitrary tangent vector

$$\Lambda(\theta_0, y_0, u_0) = \lim_{n \to \infty} \frac{\ln \| J(\theta_n, y_n, T_n) J(\theta_{n-1}, y_{n-1}, T_{n-1}) \cdots J(\theta_0, y_0, T_0) u_0) \|}{\sum_{i=1}^{n} T_i}, \tag{6}$$

where (θ_0, y_0) is the initial point on the trajectory, T_i is the time of the i-th kick such that the time between the $i+1$-th and i-th kicks is given by $T_{i+1} - T_i, i = 0, 1, 2, \ldots$, and u_0 is an arbitrary unit vector. We can see that $\Lambda(\theta_0, y_0, u_0)$ will generally depend on the initial point (θ_0, y_0) and on the direction of the unit vector u_0.

3.1 Study 1: periodically kicked oscillators

In this study, kicks of constant amplitude A were delivered to the system at constant time intervals T. Keeping with the approach from [3], for each parameter choice (σ, A, λ, T) we estimate the maximum Lyapunov exponent Λ_{max} by computing trajectories for 10 uniformly distributed initial points $(\theta_0, y_0) \in [0, 1) \times [-0.1, 0.1]$.

Each run consists of 4×10^5 iterates of the map to allow for a sufficiently precise estimate of the limit. From

the 10 computed values of Λ_{max}, we select the largest of the set.

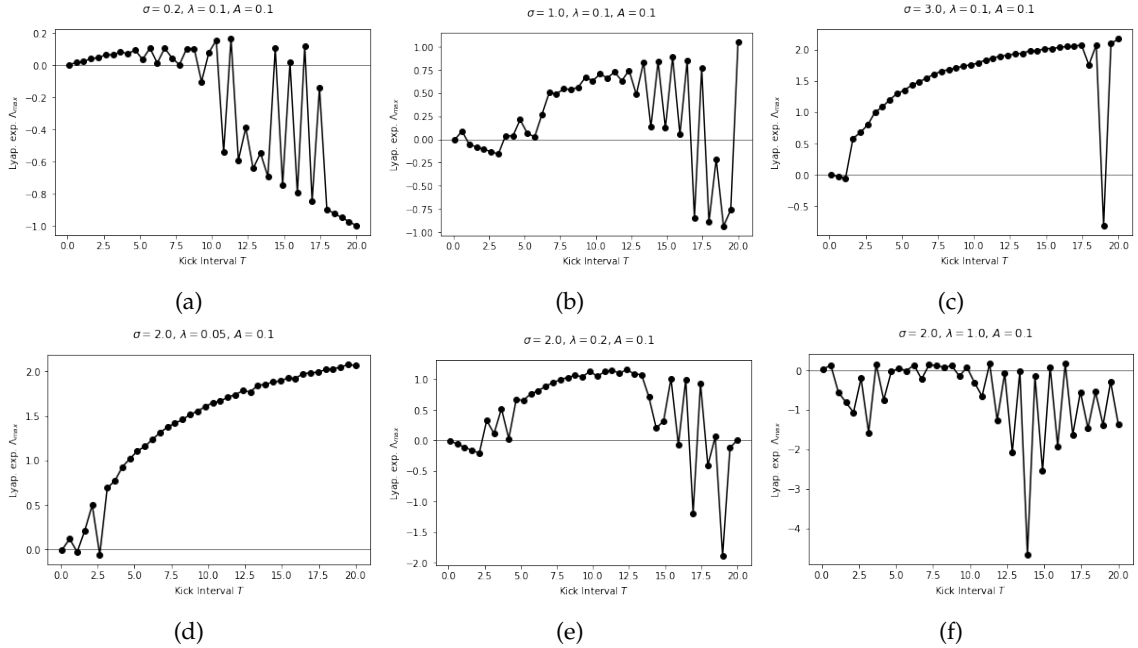

Figure 3: Recreation of graphs for Study 1. Plots (a-c) show recreations of Figure 3 from the paper (varying σ), and Plots (d-f) show recreations of Figure 4 from the paper (varying λ

Figure (3) shows our results of the reproduction. While there are some differences between our graphs and those of the authors, we draw the same conclusions as we see qualitatively similar results. For small values of $(\sigma/\lambda)A$, we are observing these wild oscillations. For $(\sigma/\lambda)A \approx 3$ and larger, we are observing positive lyapunov exponents, which means that our system is producing chaotic behavior. We are also noticing that as T increases, the maximum lyapunov exponents are also increasing.

3.2 Study 2: Poisson Kicks

In this study, the assumption of constant kick amplitudes and intervals was relaxed. Instead, kicks occur at random times with random amplitudes, and are modeled by a Poisson process with rate $\frac{1}{T}$. The system is described by

$$\begin{aligned} \dot{\theta} &= 1 + \sigma y \\ \dot{y} &= -\lambda y + \sin(2\pi\theta) \sum_n \boldsymbol{A}_n \delta(t - \boldsymbol{T}_n), \end{aligned} \tag{7}$$

where $\boldsymbol{T}_n$ are the kick times such that $T_{n+1} - T_n, n = 0, 1, 2, \ldots$ are independent and identically distributed exponential random variables with mean T, and the kick amplitudes $\boldsymbol{A}_n$ are independent and identically

distributed uniform random variables over the interval $[0.8A, 1.2A]$ for $A > 0$. All other details are identical to study 1. In subsequent sections we will explore the effects of different probability laws for $\boldsymbol{T}_n$ and $\boldsymbol{A}_n$ on the results.

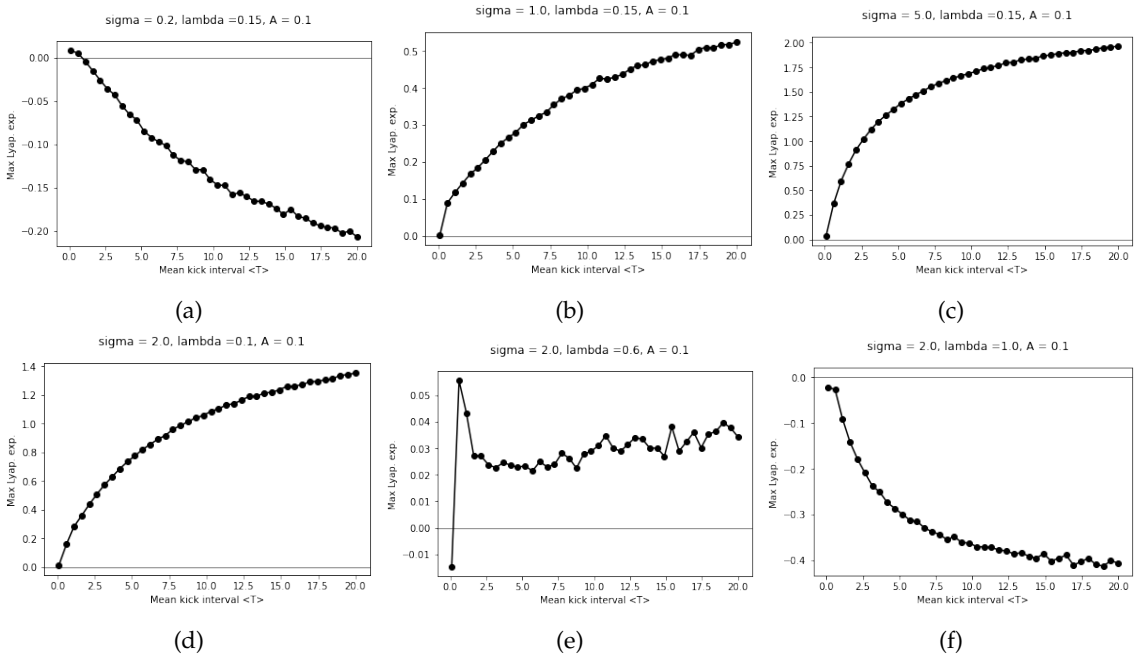

(a) (b) (c)

(d) (e) (f)

Figure 4: Recreation of Study 2 with Poisson Kicks. With Poisson kicks, the maximum lyapunov exponents converge smoothly and have chaos when $(\sigma/\lambda)A$ is large enough.

Figure (4) shows our reproduced graphs of Study 2. Like the authors, we found that the maximum lyapunov exponents converge smoothly without the wide oscillations like the periodic kicks of study 1. This is because of the averaging affects of the random kicks. We also found chaotic behavior (positive lyapunov exponents) when $(\sigma/\lambda)A$ is large enough. With randomness added, $(\sigma/\lambda)A$ also does not need to be as high as study 1 without randomness.

4 Novel Investigations and Results

4.1 Chaotic Behavior is Observed with Varied Random Distributions

Study 1 and Study 2 showed that randomness significantly affected the way that our systems behaves, and how and whether it will lead to chaos. We wanted to explore this further and explore some more how randomness affected the chaotic behavior of our system.

In Study 2, the authors explored how Poisson kicks would affect the chaotic behaviors. In this study, the

authors changed both T (the time between kicks) and A (the kick amplitude) and made them both random. In our experiments, we found that changing either T or A would lead to positive lyanpunov exponents sooner (smaller values of $(\sigma/\lambda)A$).

We also explored a variety of types of random distributions and found that a variety of types of random distributions on T will lead to smooth convergence of the maximum lyapunov exponents. These results are demonstrated in Figure (5). In these figures, you can see the original of study 1 (without any kind of randomness) in the blue, and a variety of types of disibutions including Exponential (same as study 2 but without random A), Uniform, Normal, and Cauchy. Like the results of study 2, we are observing smooth convergence, either to negative maximum lyapunov exponents when $(\sigma/\lambda)A$ is small or positive maximum lyapunov exponents when $(\sigma/\lambda)A$ is large enough.

We also found that a variety of types of disibutions on A would lead to chaotic behavior sooner, but not necessarily smoother. These results can be seen in Figure (6). We can see that for the smaller values of $(\sigma/\lambda)A$, the graphs have these oscillations, which is believed to be a product of transient chaos. This is showing that the smooth behavior we are observing in Study 2 is from the averaging affects in the kick times (T), and not necessarily the kick amplitudes. We are observing that the randomness on A is producing chaotic behavior sooner (for lower values of $(\sigma/\lambda)A$).

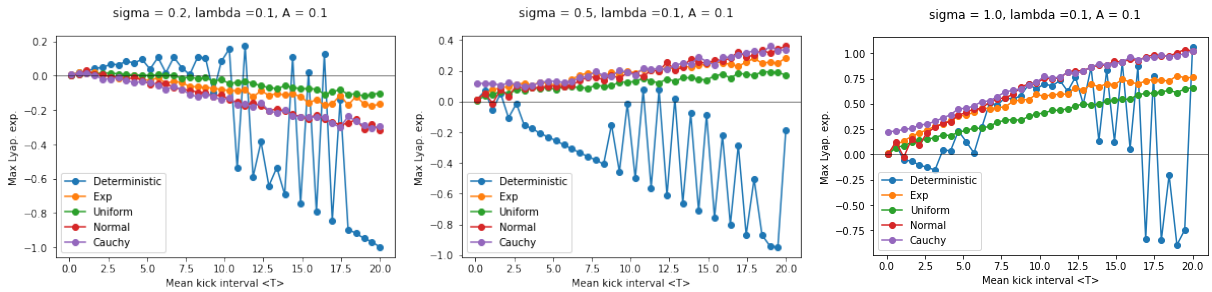

(a) (b) (c)

Figure 5: Plots representing different types of random numbers for the time between kicks. Notice how the curves are smooth for the random kicks, and chaos is observed for smaller coefficients than the periodic kicks without randomness.

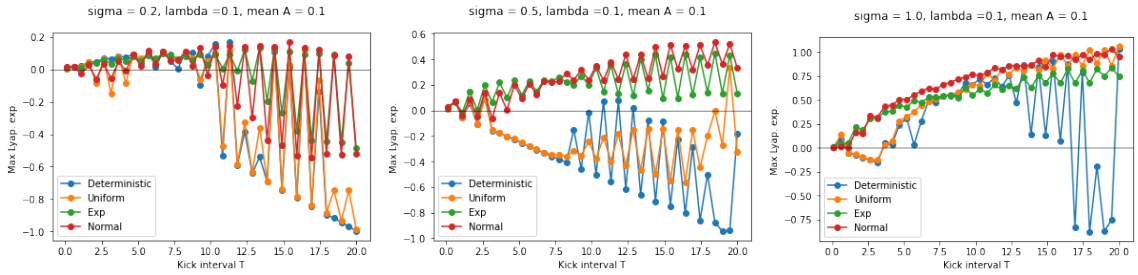

(a) (b) (c)

Figure 6: Plots of representing different types of random numbers on the amplitude of kicks

4.2 Chaotic Behavior is Observed in a Predator-Prey Model

The authors claim that applying kicks to any model with a hyperbolic limit cycle can produce chaos. Therefore, we wanted to test this claim on an ecological model with a unique hyperbolic limit cycle. We chose to study an ecological model as both periodic forcing and chaos are relevant to ecological phenomena. The model we chose is the Rosenzweig-MacArthur predator-prey model, which has been shown to have a unique hyperbolic limit cycle near the prey extinction equilibrium [1].

The equations for this model are given by the following equations

$$\begin{aligned} \frac{dx}{dt} &= x\left(1-\frac{x}{K}\right) - \frac{mxy}{1+x} \\ \frac{dy}{dt} &= \frac{mxy}{1+x} - cy \end{aligned} \tag{8}$$

where the prey experiences logistic growth with carrying capacity K and density dependent predation with rate m. The predators grow according the the predation rate and die at rate c.

To determine if applying kicks to this system produces chaos, we use a different numerical method to apply kicks and calculate the Lyapunov exponents than in [3] because we cannot find an explicit solution for this system.

Analogous to the map reduction method, we implement deterministic kicks by computing the trajectory of the system up to each kick (for intervals T), applying the kick map, and calculating the trajectory until the next kick. We calculate the trajectory for two sets of initial conditions that are infinitesimally close, on the order of 10^{-9} apart. We then find the log of the difference between these two trajectories, approximated with a polynomial of order 1, and calculate the slope of the polynomial. This slope is an approximation of the maximum Lyapunov exponent.

The results of this can be seen in Figure 7. This figure shows that chaos can be produced for some kick

maps, specifically those with $T \approx 12.5$. This supports the authors' claim that for generic systems, there exists a kick map for which chaos can be produced.

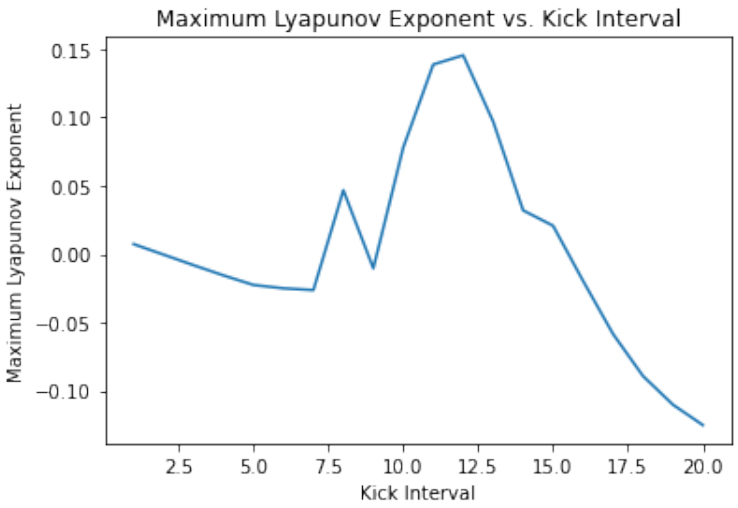

Figure 7: Maximum Lyapunov exponents of the Rosenzweig-MacArthur predator-prey model with various kick intervals

An issue we faced with this numerical method is that we could not completely reproduce the results of [3] using this new method. However, the results were qualitatively similar.

4.3 Conclusion and Discussion

In their 2008 paper, Lin and Young numerically investigated the unexpected formation of chaotic behavior in systems with hyperbolic limit cycles that undergo shear. They focused their efforts on a linear model and applied several configurations of deterministic and random kicks to the system. Their results demonstrated that chaotic behavior in such systems can be achieved for small kicks when there was a modest inbalance between shearing and damping. They also predicted that the phenomena studies should occur in many generic systems.

In this work, we have presented a brief exposition of their analytic results, illustrated with original calculations and figures, and have reproduced their numerical results for periodic kicks and Poisson random kicks. Additionally, we have expanded these numerical results by showing numerically that chaotic behavior is robust to the probability laws governing the kick amplitudes and interval between kicks. Finally, we have investigated the formation of chaotic behavior in a kicked predator-prey system. A future step in this project could include developing a robust method for calculating Lyapunov exponents in systems with periodic kicks and determining if random forcing produces chaos more consistently in the predator-prey

model.

A Code

A.1 Study 1 reproduction

[ ]:
```
# Import packages
import numpy as np
import matplotlib.pyplot as plt
import tqdm as tqdm
from decimal import *
%matplotlib inline
```

[ ]:
```
# Define Parameters
sigma = 0.2 #shear
lam = 0.1 #damping
A = 0.1 #kick amplitude
```

[ ]:
```
# Build Map reduction of dynamics: Lin. et al equation 5
def H(theta):
    return np.sin(2*np.pi*theta)

def f_map(theta,y,lam, sigma, T, A): # for theta
    return (theta + T + (sigma/lam)*(y + A*H(theta))*(1 - np.exp(-lam*T))) % 1

def g_map(theta, y, lam, T, A): # for y
    return np.exp(-lam*T)*(y + A*H(theta))
```

[ ]:
```
# Compute Jacobian of map reduction
c2 = sigma/lam

def jac1(theta, T, A):
    c3 = 2*np.pi*A*np.cos(2*np.pi*theta)
    c1 = np.exp(-lam*T)

    # see: https://docs.python.org/3/library/decimal.html
    return np.array([[Decimal((1 + c2*c3*(1-c1))), Decimal((c2*(1-c1)))],
```

```
                    [Decimal((c1*c3)), Decimal(c1)]])
```

[ ]:
```
# Run test simulations


Ts = np.linspace(0.1,20,40) #range T kicks from 0.1 to 20
sim_ly_s = []


for t in tqdm.tqdm(Ts):
    T = t # set time between kicks


    max_run = 10 # no. of replications
    max_iter = 4e5 # no. of map iterations


    run_ly_s = []


    # Run with fixed parameter values
    for i in range(max_run):


        # random initial state
        theta_T = np.random.uniform(0,1)
        y_T = np.random.uniform(-0.1, 0.1)


        # generate unit tangent vector
        u = np.array([0,1]).T
        log_arg = u # initialize log argument for lyapunov exponent


        for i in range(int(max_iter)):


            # Update jacobian product
            log_arg = jac1(theta_T, T, A).dot(log_arg)


            # Update system state: (theta,y)
```

```
            theta_T = f_map(theta_T, y_T, lam, sigma, T, A)
            y_T = g_map(theta_T, y_T, lam, T, A)

        # Store run values
        run_ly_s.append(float(Decimal(np.linalg.norm(log_arg)).ln()/(max_iter)))

    # Store max lyapunov exponents
    sim_ly_s.append(np.unique(run_ly_s)[-2]) #pick second largest
```

[ ]:
```
# Plot max lyapunov exponents
plt.plot(A_list, sim_ly_s, 'ko-')
plt.axhline(y=0, color='k', linewidth= 0.5)
plt.xlabel('A')
plt.ylabel('Max Lyap. exp.')
plt.suptitle('sigma = {}, lambda ={}, A = {}'.format(sigma,lam,A))
plt.show()
```

A.2 Study 2 Reproduction

[ ]:
```
# Import packages
import numpy as np
import matplotlib.pyplot as plt
import tqdm as tqdm
from decimal import *
from scipy.stats import cauchy
%matplotlib inline
```

[ ]:
```
# Define Parameters
sigma = 2.0 #shear
lam = 1.0 #damping
A = 0.1 #kick amplitude
```

[ ]:
```
# Build Map reduction of dynamics: Lin. et al equation 5
def H(theta):
```

```
    return np.sin(2*np.pi*theta)


def rand_T(mean_T):
    return np.random.exponential(mean_T)


def rand_T_cauchy(mode_T, scale = 1):
    rng = np.random.default_rng()
    return np.maximum(0, cauchy.rvs(loc = mode_T, scale = scale, size=1).item())


def rand_T_norm(mean_T, scale = 1):
    rng = np.random.default_rng()
    return np.maximum(0, rng.normal(loc = mean_T, scale = 1/(mean_T**2)))


def f_map(theta,y,lam, sigma, T, A): # for theta
    return (theta + T + (sigma/lam)*(y + A*H(theta))*(1 - np.exp(-lam*T))) % 1


def g_map(theta, y, lam, T, A): # for y
    return np.exp(-lam*T)*(y + A*H(theta))


rand_T_cauchy(1,1/(10**32))
```

[ ]:
```
# Compute Jacobian of map reduction
c2 = sigma/lam


def jac1(theta, T, A):
    c3 = 2*np.pi*A*np.cos(2*np.pi*theta)
    c1 = np.exp(-lam*T)


    # see: https://docs.python.org/3/library/decimal.html
    return np.array([[Decimal((1 + c2*c3*(1-c1))), Decimal((c2*(1-c1)))],
                     [Decimal((c1*c3)), Decimal(c1)]])
```

[ ]:
```
# Run test simulations


Ts = np.linspace(0.1,20,40) #mean kick interval is varying
sim_ly_s = []


for t in tqdm.tqdm(Ts):
    T = t # set time between kicks


    max_run = 10 # no. of replications
    max_iter = 4e5 # no. of map iterations


    run_ly_s = []


    # Run with fixed parameter values
    for i in range(max_run):


        # random initial state
        theta_T = np.random.uniform(0,1)
        y_T = np.random.uniform(-0.1, 0.1)


        # generate unit tangent vector
        u = np.array([0,1]).T
        log_arg = u # initialize log argument for lyapunov exponent


        for j in range(max_iter):
            # Determine time of next kick
            T_kick = rand_T(T)
            A_kick = A*np.random.uniform(0.8,1.2)


            # Update jacobian product
            log_arg = jac1(theta_T, T_kick, A_kick).dot(log_arg)
```

```
            # Update system state: (theta,y)
            theta_T = f_map(theta_T, y_T, lam, sigma, T_kick, A_kick)
            y_T = g_map(theta_T, y_T, lam, T_kick, A_kick)

        # Store run values
        run_ly_s.append(float(Decimal(np.linalg.norm(log_arg)).ln()/max_iter))

    # Store max lyapunov exponents
    sim_ly_s.append(np.unique(run_ly_s)[-2])#get seond largest
```

[ ]:
```
# Plot max lyapunov exponents
plt.plot(Ts, sim_ly_s, 'ko-')
plt.axhline(y=0, color='k', linewidth= 0.5)
plt.xlabel('Mean kick interval <T>')
plt.ylabel('Max Lyap. exp.')
plt.suptitle('sigma = {}, lambda ={}, A = {}'.format(sigma,lam,A))
plt.show()
```

A.3 Exploring different types of disutubtions.

[ ]:
```
# Import packages
import numpy as np
import matplotlib.pyplot as plt
import tqdm as tqdm
from decimal import *
%matplotlib inline
```

[ ]:
```
# Define Parameters
sigma = 1.0 #shear
lam =  0.1 #damping
A = 0.1 #kick amplitude
#T = 2 #time interval of kicks
```

[ ]:
```
# Build Map reduction of dynamics: Lin. et al equation 5
def H(theta):
    return np.sin(2*np.pi*theta)


#variety of types of disributions
def rand_T(mean_T):
    return np.random.exponential(mean_T)


def rand_T_uniform(mean_T):
    return np.random.uniform(0, mean_T)


def rand_T_gaus(mean_T):
    return np.random.normal(mean_T, mean_T/10.0)


def rand_T_deter(mean_T):
    return mean_T


def rand_T_cauchy(mode_T):
#     print(np.random.standard_cauchy() + mode_T)
    return abs(np.random.standard_cauchy() + mode_T)


def f_map(theta,y,lam, sigma, T, A): # for theta
    return (theta + T + (sigma/lam)*(y + A*H(theta))*(1 - np.exp(-lam*T))) % 1


def g_map(theta, y, lam, T, A): # for y
    return np.exp(-lam*T)*(y + A*H(theta))
```

[ ]:
```
# Compute Jacobian of map reduction
c2 = sigma/lam


def jac1(theta, T, A):
    c3 = 2*np.pi*A*np.cos(2*np.pi*theta)
    c1 = np.exp(-lam*T)
```

```
    # see: https://docs.python.org/3/library/decimal.html
    return np.array([[Decimal((1 + c2*c3*(1-c1))), Decimal((c2*(1-c1)))],
                     [Decimal((c1*c3)), Decimal(c1)]])
```

[ ]:
```
# Run test simulations
Ts = np.linspace(0.1,20,40)
def test_sim(rand_T_func, vary_A = True):

    sim_ly_s = []

    for t in tqdm.tqdm(Ts):
        T = t # set time between kicks

        max_run = 5 # no. of replications
        max_iter = 10000 # no. of map iterations

        run_ly_s = []

        # Run with fixed parameter values
        for i in range(max_run):

            # random initial state
            theta_T = np.random.uniform(0,1)
            y_T = np.random.uniform(-0.1, 0.1)

            # generate unit tangent vector
            u = np.array([0,1]).T
            log_arg = u # initialize log argument for lyapunov exponent

            for j in range(max_iter):
                    # Determine time of next kick
```

```
                T_kick = abs(rand_T_func(T))
                if vary_A:
                    A_kick = A*np.random.uniform(0.8,1.2)
                else:
                    A_kick = A

                # Update jacobian product
                try:
                    log_arg = jac1(theta_T, T_kick, A_kick).dot(log_arg)
                except:
                    print(T_kick)

                # Update system state: (theta,y)
                theta_T = f_map(theta_T, y_T, lam, sigma, T_kick, A_kick)
                y_T = g_map(theta_T, y_T, lam, T_kick, A_kick)

            # Store run values
            run_ly_s.append(float(Decimal(np.linalg.norm(log_arg)).ln()/max_iter))

        # Store max lyapunov exponents
        sim_ly_s.append(np.unique(run_ly_s)[-2])#np.max(run_ly_s))
    return sim_ly_s
```

[ ]:
```
sim_ly_s_exp = test_sim(rand_T)
# sim_ly_s_exp_b = test_sim(rand_T, vary_A = False)
# sim_ly_s_unif = test_sim(rand_T_uniform)
# sim_ly_s_unif_b = test_sim(rand_T_uniform, vary_A = False)
# sim_ly_s_deter = test_sim(rand_T_deter, vary_A = False)
# # sim_ly_s_deter_b = test_sim(rand_T_deter)
# # sim_ly_s_gaus = test_sim(rand_T_gaus)
# sim_ly_s_gaus_b = test_sim(rand_T_gaus, vary_A = False)
# sim_ly_cauchy_b = test_sim(rand_T_cauchy, vary_A = False)
```

```
[ ]: # Plot max lyapunov exponents
     # plt.plot(Ts, sim_ly_s_deter, 'o-', label = "Deterministic")
     plt.plot(Ts, sim_ly_s_exp, 'o-', c='k', label = "Exp")
     # plt.plot(Ts, sim_ly_s_exp_b, 'o-', label = "Exp")
     # # plt.plot(Ts, sim_ly_s_unif, 'o-', label = "Uniform")
     # plt.plot(Ts, sim_ly_s_unif_b, 'o-', label = "Uniform")


     # # plt.plot(Ts, sim_ly_s_deter_b, 'o-', label = "Deterministic - Varied")
     # # plt.plot(Ts, sim_ly_s_gaus, 'o-', label = "Normal")
     # plt.plot(Ts, sim_ly_s_gaus_b, 'o-', label = "Normal")
     # plt.plot(Ts, sim_ly_cauchy_b, 'o-', label = "Cauchy")
     plt.axhline(y=0, color='k', linewidth= 0.5)
     plt.xlabel('Mean kick interval <T>')
     plt.ylabel('Max Lyap. exp.')
     # plt.legend()
     plt.suptitle('sigma = {}, lambda ={}, A = {}'.format(sigma,lam,A))
     plt.show()
```

B Lin and Young Paper

References

[1] Tedra Bolger. *A Predator-Prey Model in the Chemostat with Ivlev Functional Response*. PhD thesis, 2017.

[2] Ying-Cheng Lai and Tel Tamas. *Transient chaos: complex dynamics on finite time scales*. Springer, 2011.

[3] Kevin K Lin and Lai-Sang Young. Shear-induced chaos. *Nonlinearity*, 21(5):899–922, March 2008.

[4] Qiudong Wang and Lai-Sang Young. Strange attractors with one direction of instability. *Communications in Mathematical Physics*, 218(1):1–97, April 2001.

[5] Qiudong Wang and Lai-Sang Young. Strange attractors in periodically-kicked limit cycles and hopf bifurcations. *Communications in Mathematical Physics*, 240(3):509–529, August 2003.

[6] Qiudong Wang and Lai-Sang Young Young. From invariant curves to strange attractors. *Communications in Mathematical Physics*, 225(2):275–304, February 2002.

Shear-Induced Chaos

Kevin K. Lin* and Lai-Sang Young†
Courant Institute of Mathematical Sciences
New York University

May 22, 2007

Abstract

Guided by a geometric understanding developed in earlier works of Wang and Young, we carry out some numerical studies of shear-induced chaos. The settings considered include periodic kicking of limit cycles, random kicks at Poisson times, and continuous-time driving by white noise. The forcing of a quasi-periodic model describing two coupled oscillators is also investigated. In all cases, positive Lyapunov exponents are found in suitable parameter ranges when the forcing is suitably directed.

Introduction

This paper presents a series of numerical studies which investigate the use of shear in the production of chaos. The phenomenon in question can be described roughly as follows: An external force is applied to a system with tame, nonchaotic dynamics. If the forcing is strategically applied to interact with the shearing in the underlying dynamics, it can sometimes lead to the folding of phase space, which can in turn lead to positive Lyapunov exponents for a large set of initial conditions. This phenomenon, which we call *shear-induced chaos*, occurs in a wide variety of settings, including periodically-forced oscillators. For a topic as general as this, it is difficult to compile a reasonable set of references. We have not attempted to do that, but mention that the first known observation of a form of this phenomenon was by van der Pol and van der Mark 80 years ago [21]. Other references related to our work will be mentioned as we go along.

The starting point of the present work is a series of papers by Wang and Young [22, 23, 24, 25]. In these papers, the authors devised a method for proving the existence of strange attractors and applied their techniques to some natural settings; two of their main examples are periodically-kicked oscillators and systems undergoing Hopf bifurcations. They identified a simple geometric mechanism to explain how the chaotic behavior comes about. Because of the perturbative nature

*E-mail: **klin@cims.nyu.edu**. K. L. is supported by an NSF postdoctoral fellowship.
†E-mail: **lsy@cims.nyu.edu**. L.-S. Y. is supported by a grant from the NSF.

of their analysis, however, the kicks in these results have to be followed by very long periods of relaxation. In other words, the chaos in these attractors develop on a very slow time scale. Relevant parts of the results of Wang and Young are reviewed in Sect. 1.

The aim of the present paper is to study shear-induced chaos in situations not accessible by current analytic tools. We believe that this phenomenon is widespread, meaning it occurs for large sets of parameters, and that it is robust, meaning it does not depend sensitively on the type of forcing or even background dynamics as long as certain geometric conditions are met. We validate these ideas through a series of numerical studies in which suitable parameters are systematically identified following ideas from [23] and [24]. Four separate studies are described in Sects. 2– 5. The first three studies involve an oscillator driven by different types of forcing (both deterministic and stochastic); in these studies, the unforced system is a simple linear shear flow model. In the fourth study, the unforced dynamics are that of a coupled oscillator system described by a (periodic or quasi-periodic) flow on the 2-torus.

The linear shear flow used in Studies 1–3 has been studied independently in [27] and [23]. It is the simplest system known to us that captures all the essential features of typical oscillator models relevant to shear-induced chaos. Moreover, these features appear in the system in a way that is easy to control, and the effects of varying each are easy to separate. This facilitates the interpretation of our theoretical findings in more general settings in spite of the fact that numerical studies necessarily involve specific models.

We mention that our results on shear flows are potentially applicable to a setting not discussed here, namely that of the advection and mixing of passive scalar tracers in (weakly compressible) flows.

Finally, we remark that this work exploits the interplay between deterministic and stochastic dynamics in the following way: The geometry in deterministic models are generally more clear-cut. It enables us to extract more readily the relationship between quantities and to deduce the type of results these relationships may lead. Results for stochastic models, on the other hand, tend to be more *provable* than their counterparts in deterministic models, where competing scenarios lead to very delicate dependences on parameters. Our numerical results on stochastic forcing in Studies 2–4 point clearly to the possibility of (rigorous) theorems, some versions of which, we hope, will be proved in the not too distant future.

1 Rigorous Results and Geometric Mechanism

In this section, we review some rigorous results of Wang and Young (mainly [23, 24], also [22, 25]) and the geometric mechanism for producing chaos identified in the first two of these papers. We will focus on the case of limit cycles, leaving the slightly more delicate case of supercritical Hopf bifurcations to the reader. The material summarized in this section form the starting point for the numerical investigations in the present paper.

1.1 Strange Attractors from Periodically-Kicked Limit Cycles

Consider a smooth flow Φ_t on a finite dimensional Riemannian manifold M (which can be $\mathbb{R}^d$), and let γ be a *hyperbolic limit cycle, i.e.* γ is a periodic orbit of Φ_t with the property that if we linearize the flow along γ, all of the eigenvalues associated with directions transverse to γ have strictly negative real parts. The *basin of attraction* of γ, $\mathcal{B}(\gamma)$, is the set $\{x \in M : \Phi_t(x) \to \gamma \text{ as } t \to \infty\}$. It is well known that hyperbolic limit cycles are robust, meaning small perturbations of the flow will not change its dynamical picture qualitatively.

A *periodically-kicked oscillator* is a system in which "kicks" are applied at periodic time intervals to a flow Φ_t with a hyperbolic limit cycle. For now let us think of a "kick" as a mapping $\kappa : M \to M$. If kicks are applied T units of time apart, then the time evolution of the kicked system can be captured by iterating its time-T map $F_T = \Phi_T \circ \kappa$. If there is a neighborhood $\mathcal{U}$ of γ such that $\kappa(\mathcal{U}) \subset \mathcal{B}(\gamma)$, and the relaxation time is long enough that points in $\kappa(\mathcal{U})$ return to $\mathcal{U}$, *i.e.*, $F_T(\mathcal{U}) \subset \mathcal{U}$, then $\Gamma = \cap_{n \geq 0} F_T^n(\mathcal{U})$ is an attractor for the periodically kicked system F_T. In a sense, $\Gamma = \Gamma(\kappa, T)$ is what becomes of the limit cycle γ when the oscillator is periodically kicked. Since hyperbolic limit cycles are robust, Γ is a slightly perturbed copy of γ if the kicks are weak. We call it an "invariant circle." Stronger kicks may "break" the invariant circle, leading to a more complicated invariant set. Of interest in this paper is when Γ is a strange attractor, *i.e.*, when the dynamics in $\mathcal{U}$ exhibit sustained, observable chaos.

Two theorems are stated below. Theorem 1 is an abstract result, the purpose of which is to emphasize the generality of the phenomenon. Theorem 2 discusses a concrete situation intended to make transparent the relevance of certain quantities. Let $\text{Leb}(\cdot)$ denote the Lebesgue measure of a set.

Theorem 1. [24] *Let Φ_t be a C^4 flow with a hyperbolic limit cycle γ. Then there is an open set of kick maps $\mathcal{K}$ with the following properties: For each $\kappa \in \mathcal{K}$, there is a set $\Delta = \Delta(\kappa) \subset \mathbb{R}^+$ with $\text{Leb}(\Delta) > 0$ such that for each $T \in \Delta$, Γ is a "strange attractor" of F_T.*

The term "strange attractor" in the theorem has a well-defined mathematical meaning, which we will discuss shortly. But first let us take note of the fact that this result applies to all systems with hyperbolic limit cycles, independent of dimension or other specifics of the defining equations. Second, we remark that the kicks in this theorem are very infrequent, *i.e.* $T \gg 1$, and that beyond a certain T_0, the set Δ is roughly periodic with the same period as the cycle γ.

The term "strange attractor" in Theorem 1 is used as short-hand for an attractor with a package of well defined dynamical properties. These properties were established for a class of rank-one attractors (see [22] for the 2-dimensional case; a preprint for the n-dimensional case will appear shortly). In [22, 25], the authors identified a set of conditions that implies the existence of such attractors, and the verification of the conditions in [22, 25] in the context of Theorem 1 is carried out in [24] (see also [11] and [17] for other applications of these ideas). We refer the reader to the cited papers for more details, and mention only the following three characteristics implied by the term "strange attractor" in this section.

(1) There is a set $\mathcal{V}$ of full Lebesgue measure in the basin of attraction of Γ such that orbits starting from every $x \in \mathcal{V}$ have (strictly) positive Lyapunov exponents.

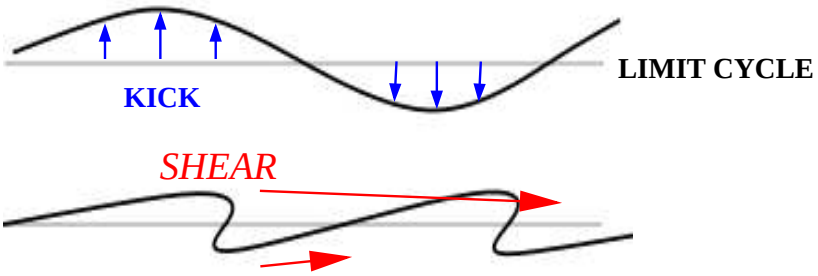

Figure 1: The stretch-and-fold action of a kick followed by relaxation in the presence of shear.

(2) F_T has an ergodic SRB measure μ, and for every continuous observable φ,

$$\frac{1}{n}\sum_{i=0}^{n-1}\varphi(F_T^i(x)) \to \int \varphi\, d\mu \qquad \text{as } n\to\infty \text{ for every } x\in\mathcal{V}.$$

(3) The system (F_T,μ) is mixing; in fact, it has exponential decay of correlations for Hölder continuous observables.

An important remark before leaving Theorem 1: Notice that the existence of "strange attractors" is asserted for F_T for only a positive measure set of T, not for all sufficiently large T. This is more a reflection of reality than a weakness of the result. For large enough T in the complement of Δ, the attractor is guaranteed to contain horseshoes, the presence of which will lead to some semblance of chaotic behavior. After a transient, however, typical orbits may (or may not) tend to a stable equilibrium. If they do, we say F_T has *transient chaos*. This is to be contrasted with properties (1)–(3) above, which represent a much stronger form of chaos.

The next result has an obvious analog in n-dimensions (see [24]), but the 2-D version illustrates the point.

Theorem 2. [24] *Consider the system*

$$\begin{aligned}\dot\theta &= 1+\sigma y\\ \dot y &= -\lambda y + A\cdot H(\theta)\cdot\textstyle\sum_{n=0}^{\infty}\delta(t-nT)\end{aligned} \tag{1}$$

where $(\theta,y)\in S^1\times\mathbb{R}$ are coordinates in the phase space, $\lambda,\sigma,A>0$ are constants, and $H: S^1\to\mathbb{R}$ is a nonconstant *smooth function. If the quantity*

$$\frac{\sigma}{\lambda}\cdot A \;\equiv\; \frac{\text{shear}}{\text{contraction rate}}\cdot \text{kick "amplitude"}$$

is sufficiently large (how large depends on the forcing function H), then there is a positive measure set $\Delta\subset\mathbb{R}^+$ such that for all $T\in\Delta$, F_T has a strange attractor in the sense above.

Here, the term involving $H(\theta)$ defines the kick, and $\gamma = S^1\times\{0\}$. We explain intuitively the significance of the quantity $\frac{\sigma}{\lambda}A$. As noted earlier, to create a strange attractor, it is necessary to

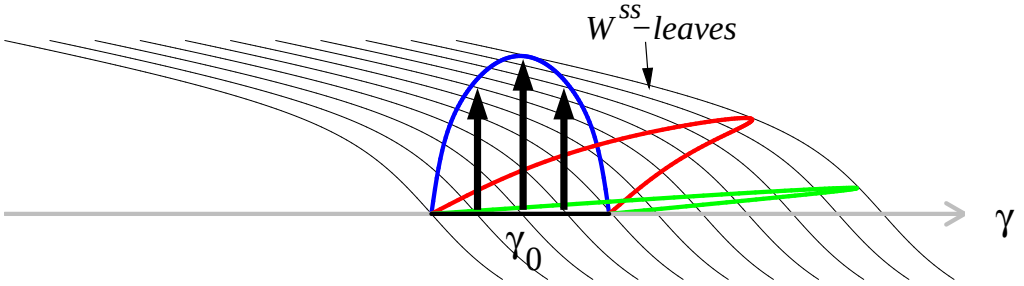

Figure 2: Geometry of folding in relation to the W^{ss}-foliation. Shown are the kicked image of a segment γ_0 and two of its subsequent images under Φ_{np}.

"break" the limit cycle. The more strongly attractive γ is, the harder it is to break. From this we see the advantage of having λ small. By the same token, a stronger forcing, *i.e.*, larger A, helps. The role of σ, the *shear*, is explained pictorially in Fig. 1: Since the function H is required to be nonconstant, let us assume the kick drives some points on the limit cycle γ up and some down, as shown. The fact that σ is positive means that points with larger y-coordinates move faster in the θ-direction. During the relaxation period, the "bumps" created by the kick are stretched as depicted. At the same time, the curve is attracted back to the limit cycle. Thus, the combination of kicks and relaxation provides a natural mechanism for repeated stretching and folding of the limit cycle. Observe that the larger the differential in speed in the θ-direction, *i.e.* the larger σ, and the slower the return to γ, *i.e.* the smaller λ, the more favorable the conditions are for this stretch-and-fold mechanism.

1.2 Geometry and Singular Limits

In Eq. (1), the quantities λ, σ and A appear naturally. But what about in general limit cycles, where the direction of the kicks vary? What, for example, will play the role of σ, or what we called shear in Eq. (1)? The aim of this subsection is to shed light on the general geometric picture, and to explain how the dynamics of F_T for large T can be understood.

Geometry of F_T and the Strong Stable Foliation

Let γ be a hyperbolic limit cycle as in the beginning of Sect. 1.1. Through each $x \in \gamma$ passes the *strong stable manifold* of x, denoted $W^{ss}(x)$ [10]. By definition, $W^{ss}(x) = \{y \in M : d(\Phi_t(y), \Phi_t(x)) \to 0 \text{ as } t \to \infty\}$; the distance between $\Phi_t(x)$ and $\Phi_t(y)$ in fact decreases exponentially. Some basic properties of strong stable manifolds are: (i) $W^{ss}(x)$ is a codimension one submanifold transversal to γ and meets γ at exactly one point, namely x; (ii) $\Phi_t(W^{ss}(x)) = W^{ss}(\Phi_t(x))$, and in particular, if the period of γ is p, then $\Phi_p(W^{ss}(x)) = W^{ss}(x)$; and (iii) the collection $\{W^{ss}(x), x \in \gamma\}$ foliates the basin of attraction of γ, that is to say, they partition the basin into hypersurfaces.

We examine next the action of the kick map κ in relation to W^{ss}-manifolds. Fig. 2 is analogous to Fig. 1; it shows the image of a segment γ_0 of γ under $F_T = \Phi_T \circ \kappa$. For illustration purposes, we assume γ_0 is kicked upward with its end points held fixed, and assume $T = np$ for some $n \in \mathbb{Z}^+$

(otherwise the picture is shifted to another part of γ but is qualitatively similar). Since Φ_{np} leaves each W^{ss}-manifold invariant, we may imagine that during relaxation, the flow "slides" each point of the curve $\kappa(\gamma_0)$ back toward γ along W^{ss}-leaves. In the situation depicted, the effect of the folding is evident.

Fig. 2 gives considerable insight into what types of kicks are conducive to the formation of strange attractors. Kicks along W^{ss}-leaves or in directions roughly parallel to the W^{ss}-leaves will not produce strange attractors, nor will kicks that essentially carry one W^{ss}-leaf to another. What causes the stretching and folding is the *variation* in how far points $x \in \gamma$ are moved by κ as measured in the direction transverse to the W^{ss}-leaves. Without attempting to give a more precise characterization, we will refer to the type of chaos that results from the geometry above as *shear-induced chaos*. We emphasize that the occurrence of shear-induced chaos relies on the interplay between the geometries of the kicks and the underlying dynamical structures.

Returning to the concrete situation of Theorem 2, since Eq. (1) without the kick term is linear, it is easy to compute strong stable manifolds. In (θ, y)-coordinates, they are lines with slope $-\lambda/\sigma$. Variations in kick distances here are guaranteed by the fact that H is nonconstant. With H fixed, it is clear that the larger σ/λ and A, the greater these variations. Note that the use of the word kick "amplitude" in the statement of Theorem 2 is a little misleading, for it is not the amplitude of the kicks *per se* that leads to the production of chaos.

Singular Limits of F_T as $T \to \infty$

When $T \gg 1$, *i.e.* when kicks are very infrequent, the map F_T sends a small tube $\mathcal{U}_T$ around γ back into itself. This is an example of what is called a *rank-one map* in [25]. Roughly speaking, a rank-one map is a smooth map whose derivative at each point is strongly contractive in all but one of the directions. Rank-one maps can be analyzed using perturbative methods if they have well-defined "singular limits." In the context of limit cycles, these singular limits do exist; they are a one-parameter family of maps $\{f_a : \gamma \circlearrowleft\}$ obtained by letting $T \to \infty$ in the following way: For each $a \in [0, p)$ (recall that $p =$ period of γ), let

$$f_a(x) \ := \ \lim_{n\to\infty} \Phi_{np+a}(\kappa(x)) \qquad \text{for all } x \in \gamma \, . \tag{2}$$

Equivalently, $f_a(x)$ is the unique point $y \in \gamma$ such that $\kappa(x) \in W^{ss}(y)$. Notice that $f_a(x) = f_0(x) + a$ (mod 1), where we identify γ with $[0, 1]$ (with the end points identified). For Eq. (1), f_a is easily computed to be

$$f_a(\theta) = \theta + a + \frac{\sigma}{\lambda} A \cdot H(\theta), \tag{3}$$

where the right side should again be interpreted as mod 1. (In the setting of driven oscillators, singular limits are sometimes known as "phase resetting curves"; they have found widespread use in *e.g.* mathematical biology [26, 9].)

It is shown in [22, 23, 24, 25] that a great deal of information on the attractor Γ of F_T for $T \gg 1$ can be recovered from these singular limit maps. The results are summarized below. These results hold generally, but as we step through the 3 cases below, it is instructive to keep in mind Eq. (1) and its singular limit (3), with $\frac{\sigma}{\lambda} A$ increasing as we go along:

(i) If f_a is injective, *i.e.*, it is a circle diffeomorphism, the attractor Γ for F_T is an invariant circle. This happens when the kicks are aimed in directions that are "unproductive" (see above), or when their effects are damped out quickly. In this case, the competing scenarios on Γ are quasi-periodicity and "sinks," *i.e.* the largest Lyapunov exponent of F_T is zero or negative.

(ii) When f_a loses its injectivity, the invariant circle is "broken". When that first happens, the expansion of the 1-D map f_a is weak, and all but a finite number of trajectories tend to sinks. This translates into a gradient type dynamics for F_T.

(iii) If f_a is sufficiently expanding away from its critical points, Γ contains horseshoes for all large T. For an open set of these T, the chaos is transient, while on a positive measure set, F_T has a strange attractor with the properties described in Sect. 1.1. These are the two known competing scenarios. (They may not account for all T.) Since $F_T \approx F_{T+np}$ for large T, both sets of parameters are roughly periodic.

The analyses in the works cited suggest that when horseshoes are first formed, the set of parameters with transient chaos is more dominant. The stronger the expansion of f_a, the larger the set of parameters with strange attractors. In the first case, the largest Lyapunov exponent of F_T may appear positive for some time (which can be arbitrarily long) before turning negative. In the second case, it stays positive indefinitely.

1.3 Limitations of Current Analytic Techniques

In hyperbolic theory, there is, at the present time, a very large discrepancy between what is thought to be true and what can be proved. Maps that are dominated by stretch-and-fold behavior are generally thought to have positive Lyapunov exponents – although this reasoning is also known to come with the following caveat: Maps whose derivatives expand in certain directions tend to contract in other directions, and unless the expanding and contracting directions are well separated (such as in Anosov systems), the contractive directions can conspire to form sinks. This is how the transient chaos described in Sect. 1.2 comes about. Still, if the expansion is sufficiently strong, one would expect that positive Lyapunov exponents are more likely to prevail – even though for any one map the outcome can go either way. *Proving* results of this type is a different matter. Few rigorous results exist for systems for which one has no *a priori* knowledge of invariant cones, and invariant cones are unlikely in shear-induced chaos.

The rigorous results reviewed in the last two subsections have the following limitations: (i) They pertain to F_T for only very large T. This is because the authors use a perturbative theory that leans heavily on the theory of 1-D maps. No non-perturbative analytic tools are currently available. (ii) A larger than necessary amount of expansion is required of the singular limit maps f_a in the proof of strange attractors. This has to do with the difficulty in locating suitable parameters called Misiurewicz points from which to perturb. (This problem can be taken care of, however, by introducing more parameters.) We point out that (i) and (ii) together exacerbate the problem: f_a is more expanding when λ is small, but if $F_T = \Phi_T \circ \kappa$ is to be near its singular limit, then $e^{-\lambda T}$ must be very small, *i.e.* λT must be very large.

That brings us to the present paper, the purpose of which is to supply numerical evidence to support some of our conjectured ideas regarding situations beyond the reach of the rigorous work reviewed. Our ideas are based on the geometry outlined in Sect. 1.2, but are not limited to periodic kicks or to the folding of limit cycles.

2 Study 1: Periodically-Kicked Oscillators

Our first model is the periodic kicking of a linear shear flow with a hyperbolic limit cycle. The setting is as in Theorem 2 with $H(\theta) = \sin(2\pi\theta)$, *i.e.*, we consider

$$\begin{array}{rcl} \dot{\theta} &=& 1 + \sigma y \ , \\ \dot{y} &=& -\lambda y + A \cdot \sin(2\pi\theta) \cdot \sum_{n=0}^{\infty} \delta(t - nT) \ , \end{array} \tag{4}$$

where $(\theta, y) \in S^1 \times \mathbb{R}$, $S^1 \equiv [0, 1]$ with the two end points of $[0, 1]$ identified. In the absence of kicks, *i.e.*, when $A = 0$, $\Phi_t(z)$ tends to the limit cycle $\gamma = S^1 \times \{0\}$ for all $z \in S^1 \times \mathbb{R}$. As before, the attractor in the kicked system is denoted by Γ. The parameters of interest are:

$$\begin{aligned} \sigma &= \text{amount of shear,} \\ \lambda &= \text{damping or rate of contraction to } S^1 \times \{0\}, \\ A &= \text{amplitude of kicks, and} \\ T &= \text{time interval between kicks.} \end{aligned}$$

Our aim here is to demonstrate that the set of parameters with chaotic behavior is considerably larger than what is guaranteed by the rigorous results reviewed in Sect. 1, and to gain some insight into this parameter set. By "chaotic behavior," we refer in this section to the property that F_T has a positive Lyapunov exponent for orbits starting from a "large" set of initial conditions, *i.e.* a set of full or nearly full Lebesgue measure in the basin of attraction of Γ. More precisely, we *assume* that such Lyapunov exponents are well defined, and proceed to compute the largest one, which we call $\Lambda_{\max}$.

We begin with some considerations relevant to the search for parameters with $\Lambda_{\max} > 0$:

(a) It is prudent, in general, to ensure that orbits do not stray too far from γ. This is because while the basin of attraction of γ in this model is the entire phase space, the basin is bounded in many other situations. We therefore try to keep $\Gamma \subset \{|y| < b\}$ with relatively small b. This is guaranteed if A is small enough that $e^{-\lambda T}(b + A) < b$; the bound is improved if, for example, no point gets kicked to maximum amplitude two consecutive iterates.

(b) Let $(\theta_T, y_T) = F_T(\theta_0, y_0)$. A simple computation gives

$$\begin{array}{rcll} \theta_T &=& \theta_0 + T + \frac{\sigma}{\lambda} \cdot [y_0 + A \sin(2\pi\theta_0)] \cdot (1 - e^{-\lambda T}) & \text{(mod 1)} \ , \\ y_T &=& e^{-\lambda T}[y_0 + A \sin(2\pi\theta_0)] \ . & \end{array} \tag{5}$$

For b relatively small, we expect the number $\frac{\sigma A}{\lambda}(1 - e^{-\lambda T})$ to be a good indicator of chaotic behavior: if it is large enough, then F_T folds the annulus $\{|y| < b\}$ with two turns and maps it into itself. The larger this number, the larger the folds, meaning the more each of the monotonic parts of the image wraps around in the θ-direction.

Summary of Findings.

(i) With the choice of parameters guided by (a) and (b) above, we find that as soon as the folding described in (b) is definite, F_T becomes "possibly chaotic", meaning $\Lambda_{\max}$ is seen numerically to oscillate (wildly) between positive and negative values as T varies. We interpret this to be due to competition between transient and sustained chaos; see (iii) in Sect. 1.2. For larger $\frac{\sigma}{\lambda}A$, i.e., as the stretching is stronger, and for T beyond an initial range, this oscillation stops and $\Lambda_{\max}$ becomes definitively positive for all the values of T computed.

(ii) As for the range of parameters with chaotic dynamics, we find that $\Lambda_{\max} > 0$ occurs under fairly modest conditions, e.g., for $\frac{\sigma}{\lambda}A = 3$, we find $\Lambda_{\max} > 0$ starting from about $T \approx 3$, which is very far from the "$T \to \infty$" in rigorous proofs. Also, while shear-induced chaos is often associated with weak damping, we find that the phenomenon occurs as well for larger λ, e.g., for $\lambda \sim 1$, provided its relation to the other parameters are favorable.

Supporting Numerical Evidence. Figures 3 and 4 show the largest Lyapunov exponent $\Lambda_{\max}$ of F_T versus the kick period T. (Note that this is the expansion rate per kick period and is T times the rate per unit time.) In Fig. 3, λ and A are fixed, and σ is increased. We purposefully start with too small a σ so that we may see clearly the gradual changes in $\Lambda_{\max}$. The results are in excellent agreement with the description at the end of Sect. 1.2 (which pertains to regimes with very large T), even though T is not so large here: In the top picture, where $\frac{\sigma}{\lambda}A$ is small, the plot confirms a competition between quasi-periodicity and sinks; in the middle picture, we see first $\Lambda_{\max}$ becoming increasingly negative, then transitions into a competition between transient and sustained chaos, with the latter dominating in the bottom picture. Fig. 4 shows the same phenomena in reverse order, with σ and A fixed and λ increasing. Notice that even for σ, λ and A leading to chaotic dynamics, $\Lambda_{\max}$ is negative for small T. This is in agreement with the influence of the factor $(1 - e^{-\lambda T})$ in Eq. (5).

As explained in (a) above, when λT is too small relative to A, orbits stray farther from γ. Data points corresponding to parameters for which this happens are marked by open squares. For purposes of demonstrating the phenomena in question, there is nothing wrong with these data points, but as explained earlier, caution must be exercised with these parameters in systems where the basin of γ is smaller.

Simulation Details. The numbers $\Lambda_{\max}$ are computed by iterating the map in Eq. (5) and its Jacobian, and tracking the rate of growth of a tangent vector. We use 4×10^5 iterates of F_T in each run. Mindful of the delicate situation due to competition between transient and sustained chaos, and to lower the possibility of atypical initial conditions, we perform 10 runs for each choice of (σ, A, λ, T), using for each run an independent, random (with uniform distribution) initial condition $(\theta_0, y_0) \in [0, 1) \times [-0.1, 0.1]$. Among the 10 values of $\Lambda_{\max}$ computed, we discard the largest and the smallest, and plot the maximum and minimum of the remaining 8. As one can see in Figs. 3 and 4, the two estimates occasionally do not agree. This may be because not all initial conditions in the system have identical Lyapunov exponents, or it may be that the convergence to the true value of $\Lambda_{\max}$ is sufficiently slow and more iterates are needed, *i.e.* there are long transients.

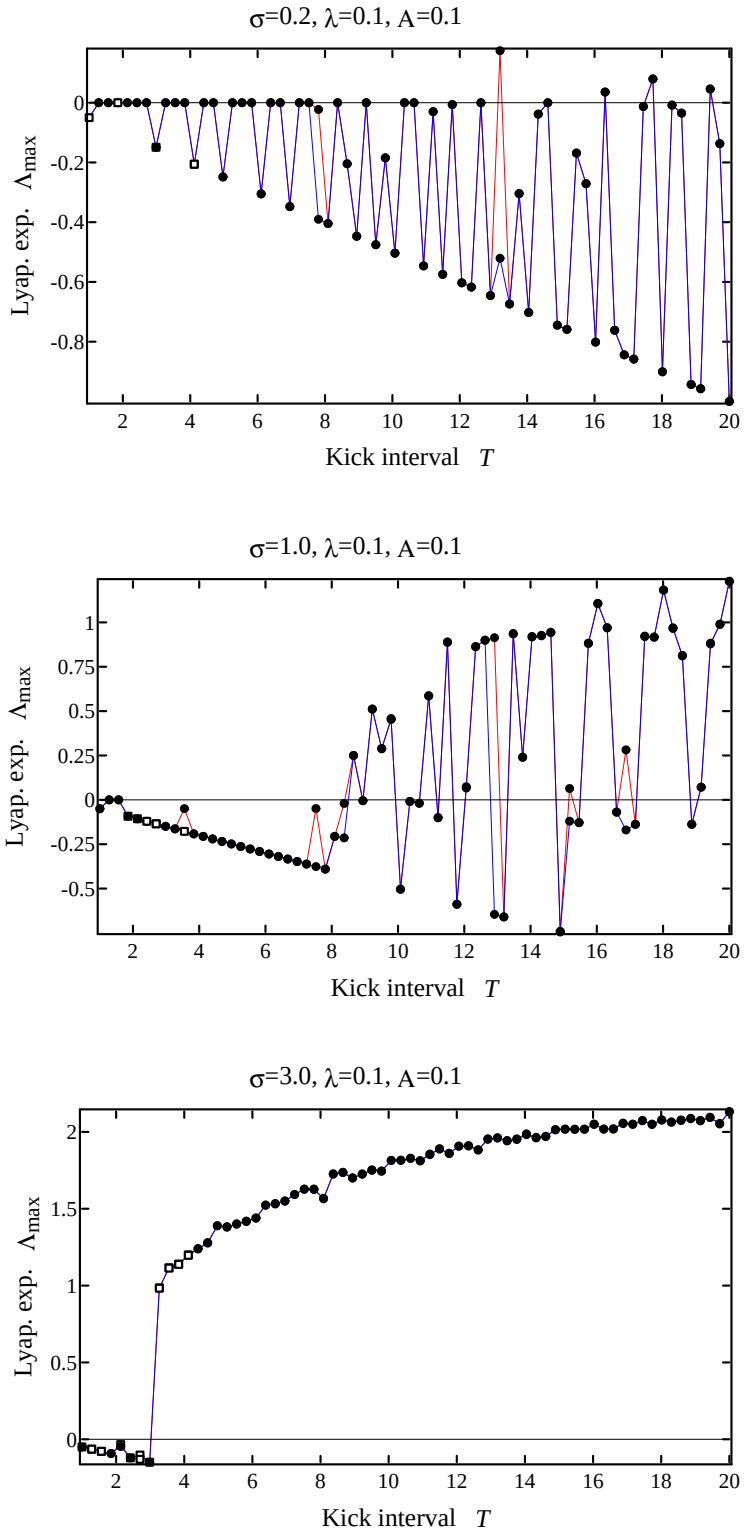

Figure 3: Effect of increasing shear on the Lyapunov exponents of the periodically-kicked linear shear flow. Squares indicate that the corresponding F_T-orbit has veered outside the region $|y| < 0.15$. Upper and lower estimates of $\Lambda_{\max}$ are both shown (see Simulation Details).

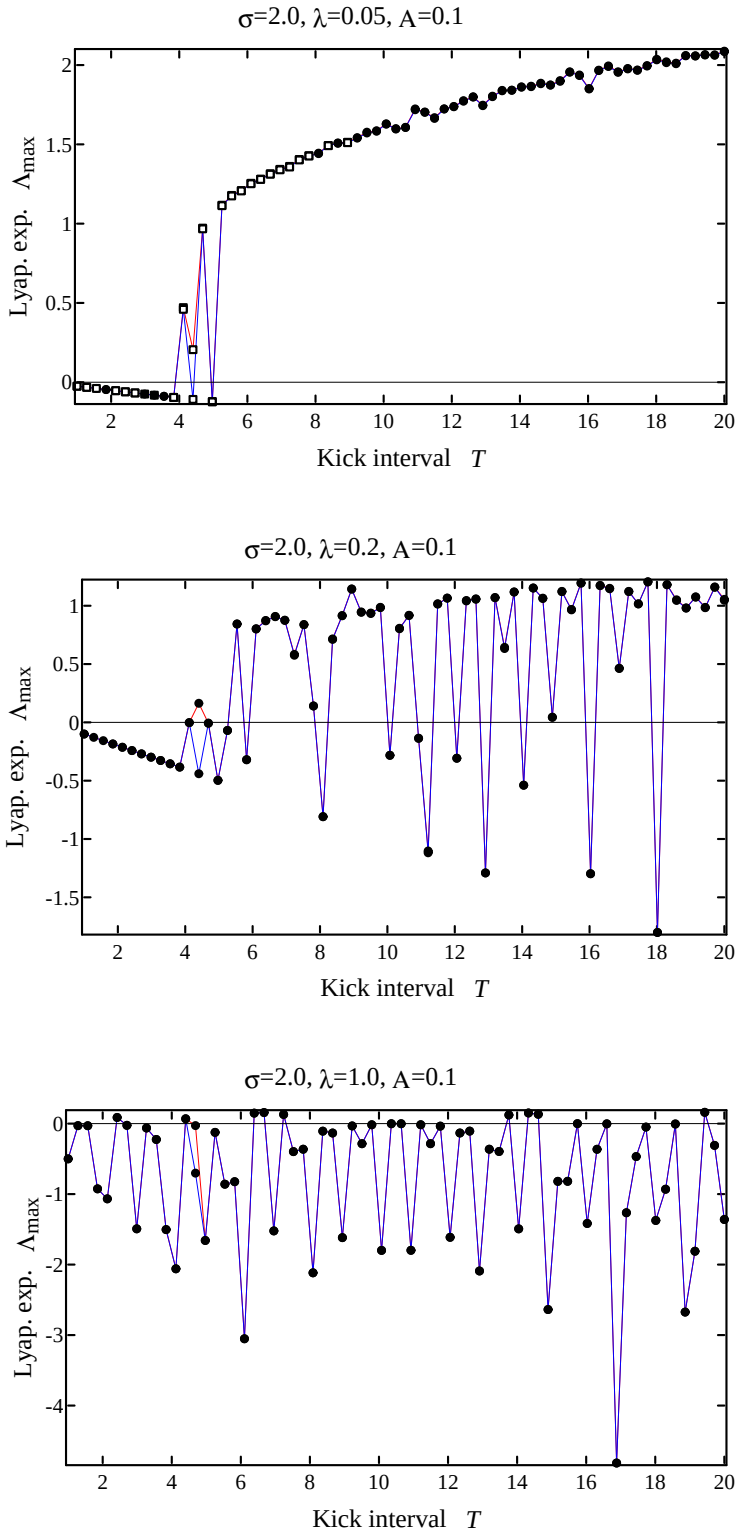

Figure 4: Effect of increasing damping on the Lyapunov exponents of the periodically-kicked linear shear flow. Squares indicate that the corresponding F_T-orbit has veered outside the region $|y| < 0.15$.

3 Study 2: Poisson Kicks

We consider next a variant of Eq. (4) in which deterministic, periodic kicks are replaced by "random kicks." Here, random kicks refer to kicks at random times and with random amplitudes. More precisely, we consider

$$\begin{aligned} \dot{\theta} &= 1 + \sigma y \\ \dot{y} &= -\lambda y + \sin(2\pi\theta) \sum_n \mathbf{A}_n \delta(t - \mathbf{T}_n) \end{aligned} \tag{6}$$

where the kick times $\mathbf{T}_n$ are such that $\mathbf{T}_{n+1} - \mathbf{T}_n$, $n = 0, 1, 2, \cdots$, are independent exponential random variables with mean T, and the kick amplitudes $\mathbf{A}_n$ are independent and uniformly distributed over the interval $[0.8\ A, 1.2\ A]$ for some $A > 0$. (We do not believe detailed properties of the laws of $\mathbf{T}$ and $\mathbf{A}$ have a significant impact on the phenomena being addressed.) The analog here of the time-T map in Study 1 is the *random map* $F = \Phi_{\mathbf{T}} \circ K_{\mathbf{A}}$ where $\mathbf{T}$ and $\mathbf{A}$ are random variables.

By the standard theory of random maps, Lyapunov exponents with respect to stationary measures are well defined and are nonrandom, *i.e.* they do not depend on the sample path taken [12]. Notice that if $\sigma \neq 0$, the system (6) has a unique stationary measure which is absolutely continuous with respect to Lebesgue measure on $S^1 \times \mathbb{R}$: starting from almost every $z_0 \in S^1 \times \mathbb{R}$, after one kick, the distribution acquires a density in the y-direction; since vertical lines become slanted under Φ_t due to $\sigma \neq 0$, after a second kick the distribution acquires a (two-dimensional) density.

In terms of overall trends, our assessment of the likelihood of chaotic behavior follows the analysis in Study 1 and will not be repeated. We identify the following two important differences:

(a) *Smooth dependence on parameters.* Due to the averaging effects of randomness, we expect Lyapunov exponents to vary smoothly with parameter, without the wild oscillations in the deterministic case.

(b) *Effects of large deviations.* A large number of kicks occurring in quick succession may have the following effects:

  (i) They can cause some orbits to stray far away from $\gamma = S^1 \times \{0\}$. This is guaranteed to happen, though infrequently, in the long run. Thus, it is reasonable to require only that a large fraction — not all — of the stationary measure (or perhaps of the *random attractors* Γ_ω) to lie in a prescribed neighborhood of γ.

  (ii) It appears possible, in principle, for a rapid burst of kicks to lead to chaotic behavior even in situations where the shear is mild and kick amplitudes are small. To picture this, imagine a sequence of kicks sending (or maintaining) a segment far from γ, allowing the shear to act on it for an uncharacteristically long time. One can also think of such bursts as effectively setting λ to near 0 temporarily, creating a very large $\frac{\sigma}{\lambda}A$. On the other hand, if σ is small, then other forces in the system may try to coax the system to form sinks between these infrequent events. We do not have the means to assess which scenario will prevail.

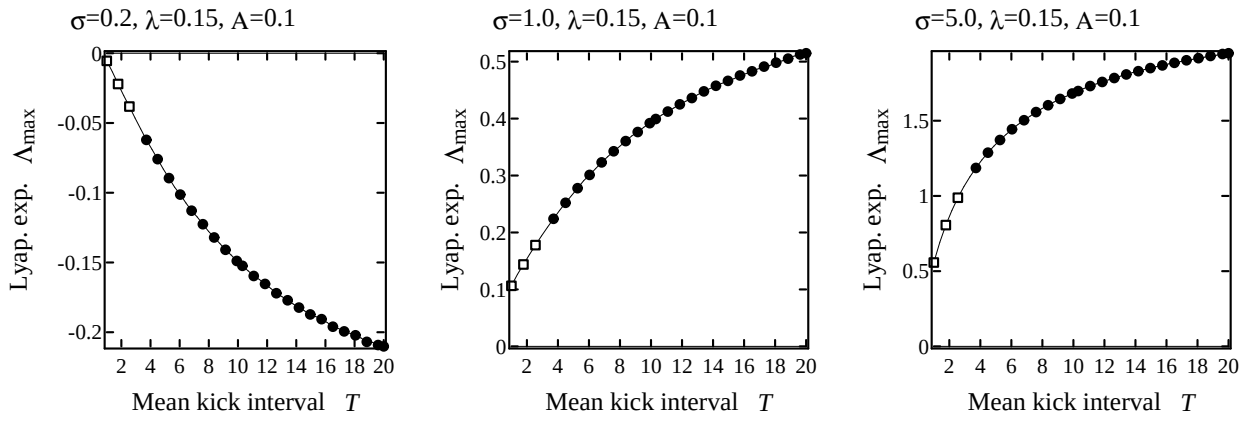

(a) *Increasing shear*

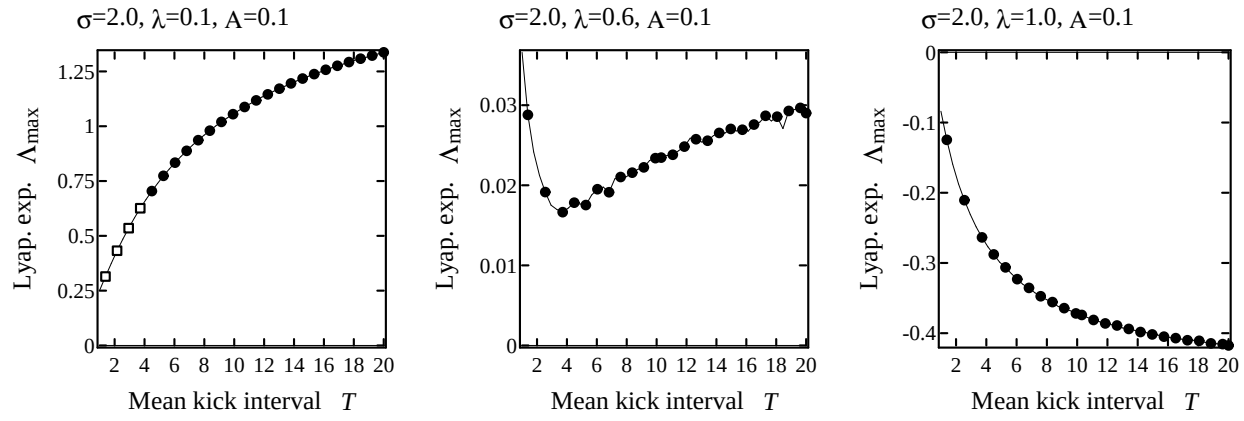

(b) *Increasing damping*

Figure 5: Lyapunov exponents for the linear shear flow with Poisson kicks. Squares indicate the corresponding orbit spends more than 20% of the time in the region $|y| > 0.1$.

Summary of Findings. *In terms of overall trends, the results are consistent with those in Study 1. Two differences are observed. One is the rapid convergence of $\Lambda_{\max}$ and their smooth dependence on parameters. The other is that positive Lyapunov exponents for F are found both for smaller values of $\frac{\sigma}{\lambda}A$ and for apparently very small T (which is impossible for periodic kicks), lending credence to the scenario described in (b)(ii) above.*

Supporting Numerical Evidence. Fig. 5 shows $\Lambda_{\max}$ as a function of the mean kick interval T. As in Study 1, we first show the effects of increasing σ and then the effects of increasing λ. Without the oscillations seen previously, the present plots are straightforward to interpret. In case one wonders how $\Lambda_{\max}$ curves can switch from strictly-decreasing to strictly-increasing behavior, the middle panel of Fig. 5(b) catches such a swtich "in the act." Squares indicate that the orbit computed spends $> 20\%$ of its time outside of the region $\{|y| < 0.1\}$.

4 Study 3: Continuous-Time Stochastic Forcing

In this section, we investigate the effect of forcing by white noise. The resulting systems are described by stochastic differential equations (SDEs). We consider two ways to force the system:

Study 3a: Degenerate white noise applied in chosen direction:

$$\begin{aligned} d\theta &= (1+\sigma y)\,dt \\ dy &= -\lambda y\,dt + a\sin(2\pi\theta)\,dB_t \end{aligned} \tag{7}$$

Study 3b: Isotropic white noise:

$$\begin{aligned} d\theta &= (1+\sigma y)\,dt + a\sin(2\pi\theta)\,dB_t^1 \\ dy &= -\lambda y\,dt + a\sin(2\pi\theta)\,dB_t^2 \end{aligned} \tag{8}$$

In Study 3a, B_t is standard 1-dimensional Brownian motion (meaning with variance $= 1$). In Study 3b, (B_t^1, B_t^2) is a standard 2-D Brownian motion, *i.e.*, they are independent standard 1-D Brownian motions. For definiteness, we assume the stochastic terms are of Itô type. Notice that the two parameters A and T in Studies 1 and 2 have been combined into one, namely a, the coefficient of the Brownian noise.

By standard theory [1, 13], the solution process of an SDE can be represented as a stochastic flow of diffemorphisms. More precisely, if the coefficients of the SDE are time-independent, then for any time step $\Delta t > 0$, the solution may be realized, sample path by sample path, as the composition of random diffeomorphisms $\cdots \circ f_3 \circ f_2 \circ f_1$, where the f_i are chosen *i.i.d.* with a law determined by the system (the f_i are time-Δt flow-maps following this sample path). This representation enables us to treat an SDE as a *random dynamical system* and to use its Lyapunov exponents as an indicator of chaotic behavior. It is clear that system (8) has a unique invariant density, which is the solution of the Fokker-Planck equation. Even though the stochastic term in system (7) is degenerate, for the same reasons discussed in Study 3, it too has a unique stationary measure, and this measure has a density. The Lyapunov exponents considered in this section are with respect to these stationary measures.

Before proceeding to an investigation of the two systems above, we first comment on the case of purely additive noise, *i.e.* Eq. (8) without the $\sin(2\pi\theta)$ factor in either Brownian term. In this case it is easy to see that all Lyapunov exponents are ≤ 0, for the random maps are approximately time-Δt maps of the unforced flow composed with random (rigid) translations. Such a system is clearly not chaotic.

With regard to system (7), we believe that even though the quantitative estimates from Study 1 no longer apply, a good part of the *qualitative reasoning* behind the arguments continues to be valid. In particular, we conjecture that

(a) trends, including qualitative dependences on σ and λ, are as in the previous two studies;

(b) the effects of large deviations noted for Poisson kicks (Study 2, item (b)) are even more prominent here, given that the forcing now occurs continuously in time.

As for system (8), we expect it to be less effective in producing chaos, *i.e.* more inclined to form sinks, than system (7). This expectation is based on the following reasoning: Suppose first that we force *only* in the θ-direction, *i.e.*, suppose the dB_t^2 term in (8) is absent. Then the stochastic flow leaves invariant the circle $S^1 \times \{0\}$, which is the limit cycle of the deterministic part of the system. A general theorem tells us that when a random dynamical system on a circle has an invariant density, its Lyapunov exponent is always ≤ 0; in this case, it is in fact strictly negative because of the inhomogeneity caused by the sine function [12]. Thus the corresponding 2-D system has "random sinks." Now let us put the y-component of the forcing back into the system. We have seen from previous studies that forcing the y direction alone may lead to chaotic behavior. The tendency to form sinks due to forcing in the θ-direction persists, however, and weakens the effect of the shear-induced stretching.

We now discuss the results of simulations performed to validate these ideas.

Summary of Findings.

(i) In the case of degenerate *white noise, the qualitative dependence of $\Lambda_{\max}$ on σ and λ are as expected, and the effects of large deviations are evident. In particular, $\Lambda_{\max}$ is positive for very small values of σ, λ and a provided $\frac{\sigma}{\lambda}$ is large.* This cannot happen for periodic kicks; we attribute it to the effect of large deviations.

(ii) Isotropic white noise is considerably less effective in producing chaos than forcing in the y-direction only, meaning it produces a smaller (or more negative) $\Lambda_{\max}$.

(iii) In both cases, we discover the following approximate scaling: Under the scaling transformations $\lambda \mapsto k\lambda, \sigma \mapsto k\sigma$ and $a \mapsto \sqrt{k}a$, $\Lambda_{\max}$ transforms approximately as $\Lambda_{\max} \mapsto k\Lambda_{\max}$. In the case of degenerate white noise, when both σ and $\frac{\lambda}{\sigma}$ are not too small (e.g., > 3), this scaling gives excellent predictions of $\Lambda_{\max}$ for the values computed.

We remark that (iii) does not follow by scaling time in the SDE. Indeed, scaling time by k in Eq. (7), we obtain

$$\begin{aligned} d\theta &= (k + k\sigma y)\, dt\,, \\ dy &= -k\lambda y\, dt + \sqrt{k}a \sin(2\pi\theta)\, dB_t\,. \end{aligned} \tag{9}$$

Thus the approximate scaling in (iii) asserts that the Lyapunov exponent of system (9), equivalently k times the $\Lambda_{\max}$ for Eq. (7), is roughly equal to that of the system obtained by changing the first equation in (9) to $d\theta = (1 + k\sigma y)dt$. In other words, $\Lambda_{\max}$ seems only to depend minimally on the frequency of the limit cycle in the unforced system.

Supporting Numerical Evidence. Plots of $\Lambda_{\max}$ as functions of a are shown in Figs. 6 – 9.

In Fig. 6, the forcing is degenerate, and for fixed σ, $\Lambda_{\max}$ decreases with increasing damping as expected. Notice that compared to the two previous studies, a somewhat larger damping is required to maintain a good fraction of the attractor near γ.

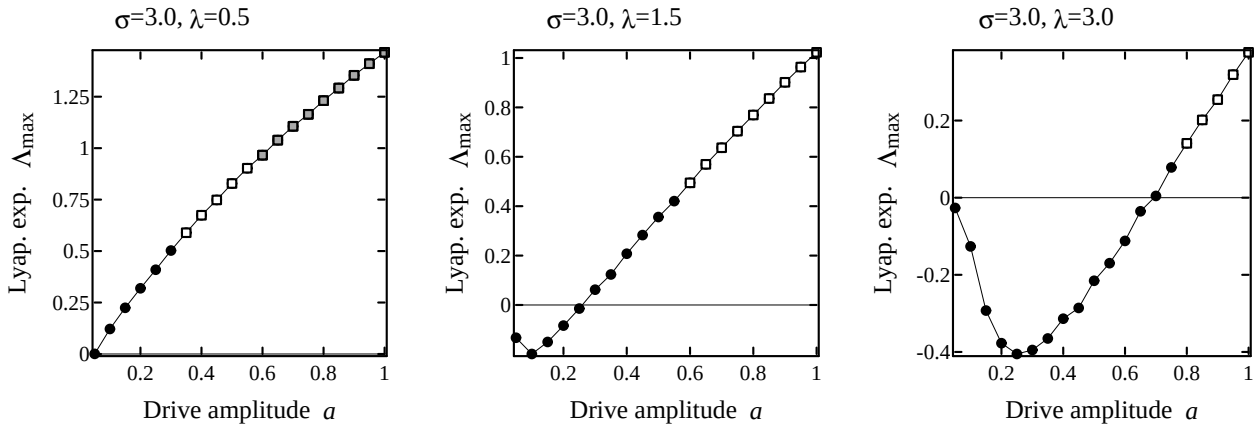

Figure 6: Lyapunov exponents for the linear shear flow driven by degenerate white noise (Eq. (7)). Open squares indicate that the corresponding orbits spend more than 20% of the time in the region $|y| > 0.3$; shaded squares do the same for the region $|y| > 0.5$.

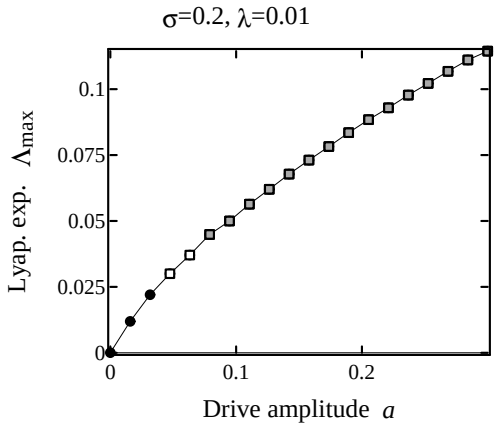

Figure 7: Lyapunov exponents for the linear shear flow driven by degnerate white noise, for small values of σ and λ.

Fig. 7 shows that $\Lambda_{\max}$ is positive for values of σ and λ as small as 0.2 and 0.01, and white noise amplitudes a close to 0. Notice first that this is consistent with the scaling conjectured in (iii) above, and second that in the case of periodic kicks, comparable values of σ and λ would require a fairly substantial kick, not to mention long relaxation periods, before chaotic behavior can be produced. We regard this as convincing evidence of the significant effects of large deviations in continuous-time forcing. (It must be pointed out, however, that in our system, the basin of attraction is the entire phase space, and a great deal of stretching is created when $|y|$ is large. That means system (7) takes greater advantage of large deviations than can be expected ordinarily.

Fig. 8(a) shows $\Lambda_{\max}$ in the isotropic case for the same parameters as in Fig. 6. A comparison of the two sets of results confirms the conjectured tendency toward negative exponents when the forcing is isotropic. Fig. 8(b) shows that this tendency can be overcome by increasing σ.

Fig. 9 shows four sets of results, overlaid on one another, demonstrating the scaling discussed

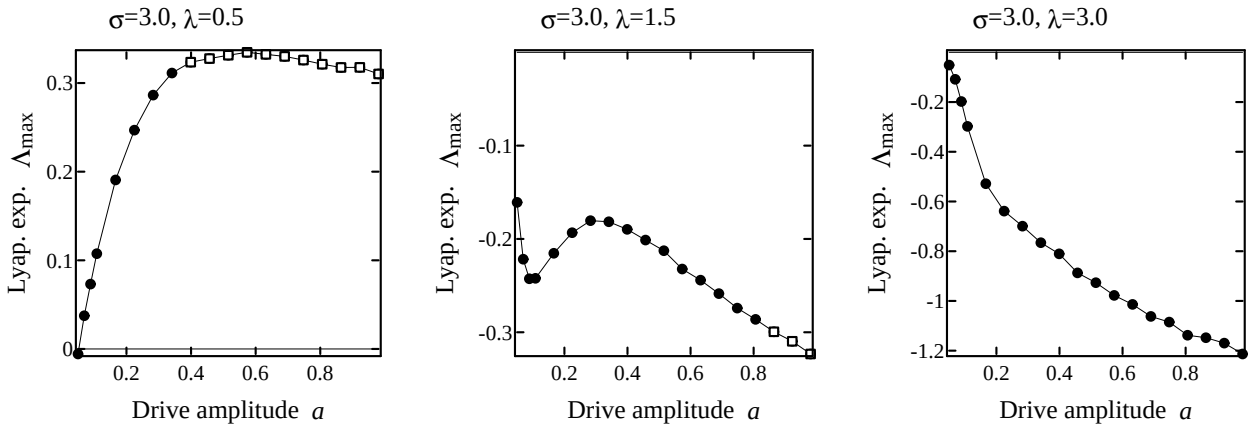

(a) $\sigma = 3.0$

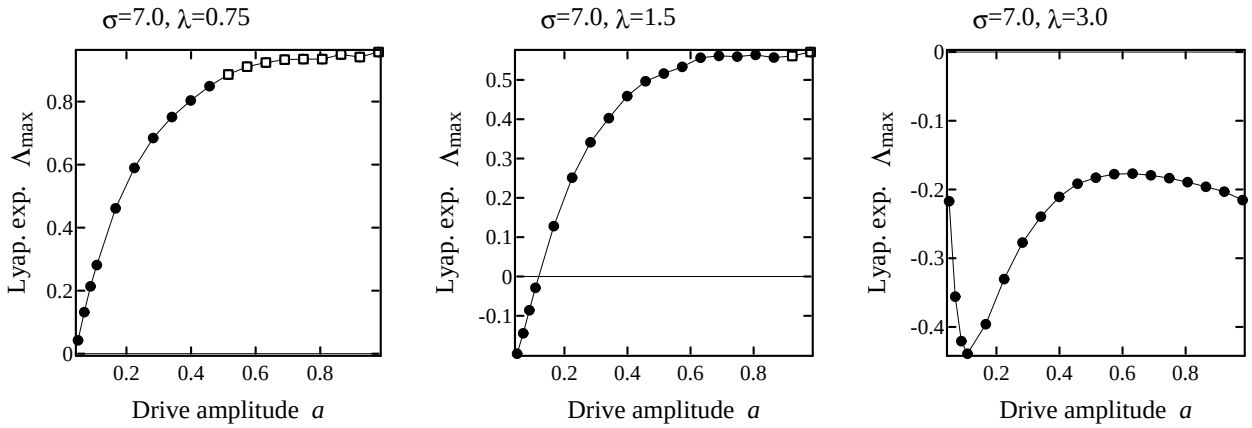

(b) $\sigma = 7.0$

Figure 8: Lyapunov exponent for the linear shear flow driven by isotropic white noise (Eq. (8)). Squares indicate that the corresponding orbits spend more than 20% of the time in the region $|y| > 0.3$.

in item (iii) above. Fixing $\frac{\sigma}{\lambda} = 6$, we show the graphs of $\Lambda_{\max}/\sigma$ as functions of $a/\sqrt{\sigma}$ for four values of σ. The top two curves (corresponding to $\sigma = 6$ and 9) coincide nearly perfectly. Similar approximate scalings, less exact, are observed for smaller values of $\frac{\sigma}{\lambda}$, both when $\Lambda_{\max}$ is positive and negative.

Simulation Details. We compute Lyapunov exponents numerically by solving the corresponding variational equations (using an Euler solver with time steps of 10^{-5}) and tracking the growth rate of a tangent vector. To account for the impact of the realization of the forcing on the computed exponents, for each choice of (σ, λ, a) we perform 12 runs in total, using 3 independent realizations of the forcing and, for each realization, 4 independent initial conditions (again uniformly-distributed in $[0, 1) \times [-0.1, 0.1]$). For almost all the parameter values, the estimates agree to fairly high accuracy, so we simply average over initial conditions and plot the result.

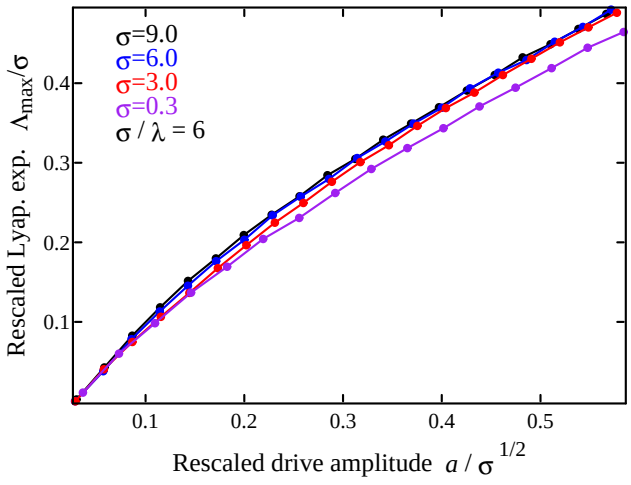

Figure 9: Evidence of scaling: We fix $\frac{\sigma}{\lambda}$ and plot $\Lambda_{\max}/\sigma$ as functions of the rescaled drive amplitude $a/\sqrt{\sigma}$; from top to bottom, the curves are in order of decreasing σ.

Related Results. The asymptotic stability of dynamical systems driven by random forcing has been investigated by many authors using both numerical and analytic methods. Particularly relevant to our study are results pertaining to the random forcing of oscillators (such as Duffing-van der Pol oscillators) and stochastic Hopf bifurcations; see e.g. [2, 3, 7, 5, 6, 8, 18, 16]. Most of the existing results are perturbative, *i.e.*, they treat regimes in which both the noise and the damping are very small. Positive Lyapunov exponents are found under certain conditions. We do not know at this point if the geometric ideas of this paper provide explanations for these results.

5 Study 4: Sheared-Induced Chaos in Quasiperiodic Flows

Model and Background Information

In this section, we will show that external forcing can lead to shear-induced chaos in a coupled phase oscillator system of the form

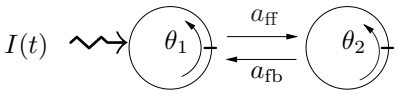

The governing equations are

$$\begin{aligned} \dot{\theta}_1 &= \nu_1 + z(\theta_1)[a_{\rm ff} g(\theta_2) + I(t)] \,, \\ \dot{\theta}_2 &= \nu_2 + z(\theta_2)[a_{\rm fb} g(\theta_1)]. \end{aligned} \tag{10}$$

The state of the system is specified by two angles, (θ_1, θ_2), so that the phase space is the torus $\mathbb{T}^2 \equiv [0,1)^2$. The constants ν_1 and ν_2 are the oscillators' intrinsic frequencies; we set $\nu_1 = 1$ and $\nu_2 = 1.1$ (representing similar but not identical frequencies). The constants $a_{\rm ff}$ and $a_{\rm fb}$ govern the strengths of the feedforward and feedback couplings. The oscillators are pulse-coupled: the coupling is

mediated by a bump function g supported on $[-\frac{1}{20}, \frac{1}{20}]$ and normalized so that $\int_0^1 g(\theta)\, d\theta = 1$. The function $z(\theta)$, which we take to be $z(\theta) = \frac{1}{2\pi}[1 - \cos(2\pi\theta)]$, specifies the sensitivity of the oscillators to perturbations when in phase θ. Finally, we drive the system with an external forcing $I(t)$, which is applied to only the first oscillator. This simple model arises from neuroscience [26, 20] and is examined in more detail in [15].

Let Φ_t denote the flow of the unforced system, *i.e.*, with $I(t) \equiv 0$. Flowlines are roughly northeasterly and are linear except in the strips $\{|\theta_1| < \frac{1}{20}\}$ and $\{|\theta_2| < \frac{1}{20}\}$, where they are bent according to the prescribed values of a_{ff} and a_{fb}. Let ρ denote the rotation number of the first return map of Φ_t to the cross-section $\{\theta_2 = 0\}$. It is shown in [14] that for $a_{\text{ff}} = 1$, ρ is monotonically increasing (constant on extremely short intervals) as one increases a_{fb}, until it reaches 1 at $a_{\text{fb}} = a_{\text{fb}}^* \approx 1.4$, after which it remains constant on a large interval. At $a_{\text{fb}} = a_{\text{fb}}^*$, a limit cycle emerges in which each oscillator completes one rotation per period; we say the system is 1:1 phase-locked, or simply *phase-locked*. In [14], it is shown numerically that forcing the system by white noise after the onset of phase-locking leads to $\Lambda_{\max} > 0$. The authors of [14] further cite Wang-Young theory (the material reviewed in Sect. 1) as a geometric explanation for this phenomenon.

In this section, we provide geometric and numerical evidence of shear-induced chaos both before and after the onset of phase-locking at $a_{\text{fb}} = a_{\text{fb}}^*$. Our results for $a_{\text{fb}} > a_{\text{fb}}^*$ support the assertions in [14]. For $a_{\text{fb}} < a_{\text{fb}}^*$, they will show that *limit cycles are not preconditions for shear-induced chaos*. We will show that in Eq. (10), the mechanism for folding is already in place before the onset of phase-locking, where the system is quasi-periodic or has periodic orbits of very long periods; the distinction between these two situations is immaterial since we are concerned primarily with finite-time dynamics. In the rest of this section, we will, for simplicity, refer to the regime prior to the onset of phase-locking as "near-periodic."

Folding: Geometric Evidence of Chaos

The dynamical picture of kicks followed by a period of relaxation has a simpler, more clear-cut geometry than that of continuous, random forcing. Thus we use the former to demonstrate why one may expect chaotic behavior over the parameter ranges in question. The kick map is denoted by κ as in Section 1.

*Folding in the periodic (*i.e. *phase-locked) regime.* We will use $a_{\text{fb}} = 1.47$ for illustration purposes; similar behavior is observed over a range of a_{fb} from 1.4 to 1.6. Note that the system is phase-locked for a considerably larger interval beyond $a_{\text{fb}} = 1.6$, but the strength of attraction grows with increasing a_{fb}, and when the attraction becomes too strong, it is harder for folding to occur.

Fig. 10 shows the limit cycle γ (*blue curve*) of the unforced system at $a_{\text{fb}} = 1.47$; more precisely, it shows a "lift" of γ to $\mathbb{R}^2$, identifying the torus $\mathbb{T}^2$ with $\mathbb{R}^2/\mathbb{Z}^2$. Also shown is the image $\kappa(\gamma)$ of the cycle after a single kick (*red curve*), where the kick map κ corresponds to $I(t) = A\sum_n \delta(t - nT)$ with $A = 1.5$, *i.e.* κ is given by $\kappa = \lim_{\varepsilon\to 0} \kappa_\varepsilon(\varepsilon)$ where $\kappa_\varepsilon(t)$ is the solution of $\dot\theta_1 = \frac{A}{\varepsilon} z(\theta_1), \dot\theta_2 = 0$. Notice the special form of the kicks: κ acts horizontally, and does not move points on $\theta_1 = 0$. In particular, κ fixes a unique point $(0, b)$ on the cycle; this point is, in fact, not affected by *any* kick of the form considered in Eq. (10). Several segments of strong stable

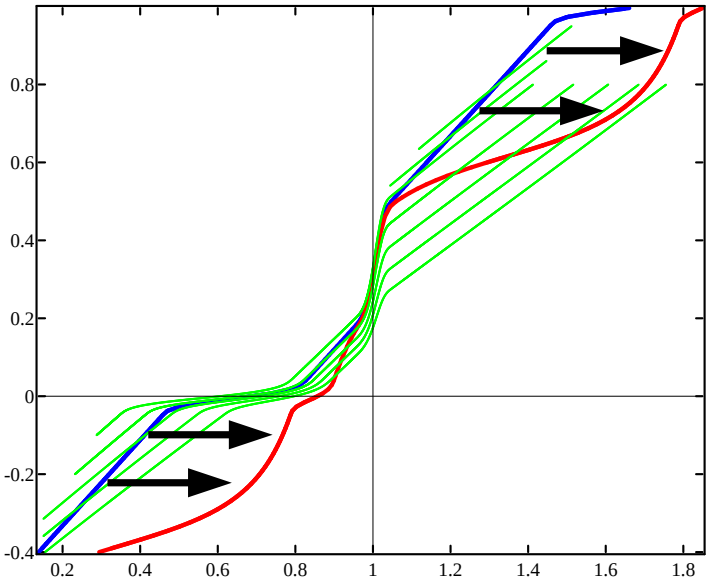

Figure 10: The strong-stable foliation of the system (10) in the phase-locked regime. *Blue:* a lift of the limit cycle. *Red:* the image of the cycle after a single kick. *Green:* strong-stable foliation. Here, the parameters are $\nu_1 = 1$, $\nu_2 = 1.1$, $a_{\text{ff}} = 1$, and $a_{\text{fb}} = 1.47$.

manifolds (*green curves*) of the unforced system are drawn. Recall that if p is the period of cycle and $n \in \mathbb{Z}^+$, then $\Phi_{np}(\kappa(z))$ lies on the W^{ss}-curve through $\kappa(z)$ and is pulled toward the cycle as n increases (see Sect. 1.2). From the relation between the W^{ss}-curves and the cycle, we see that for $z \in \gamma$, $\Phi_t(\kappa(z))$ will lag behind $\Phi_t(z)$ during the relaxation period. Notice in particular that there are points on $\kappa(\gamma)$ above the line $\theta_2 = b$ that are pulled toward the part of γ below $\theta_2 = b$. Since $(0, b)$ stays put, we deduce that some degree of folding will occur if the time interval between kicks is sufficiently long.

Fig. 11 illustrates how this folding happens through three snapshots. We begin with a segment $\gamma_0 \subset \gamma$ between $\theta_2 = 0$ and $\theta_2 = 1$ (*blue curve*) and its image after a single kick (*red curve*). Both curves are then evolved forward in time and their images at $t = 2.5$ and $t = 3.5$ are shown. The purple dot marks the point on γ_0 which does not move when kicked. Notice that these pictures are shown in a *moving frame* to emphasize the geometry of $\Phi_t(\kappa(\gamma_0))$ relative to $\Phi_t(\gamma_0)$.

Folding in the near-periodic regime. Fig. 12 shows snapshots of a similar kind for $a_{\text{fb}} = 1.2$; this value of a_{fb} puts the system in the near-periodic regime. The snapshots begin with an (arbitrary) orbit segment γ_0 and its image $\kappa(\gamma_0)$; the location of γ_0 is near that of the limit cycle in Fig. 10. The kicked segment clearly folds; indeed, the picture is qualitatively very similar to that of the limit cycle case. Note that at $a_{\text{fb}} = 1.2$, the rotation number of the return map to $\{\theta_2 = 0\}$ is a little below 1, so that $\Phi_t(\kappa(\gamma_0))$ has an overall, slow drift to the left when viewed in the fixed frame $[0, 1)^2$. This slow, left-ward drift is not especially relevant in our moving frame (which focuses on the movement of $\Phi_t(\kappa(\gamma_0))$ relative to that of $\Phi_t(\gamma_0)$). On successive laps around the torus, the orbit in question returns to the part of the torus shown in the figure, and the sequence of actions depicted in Fig. 12 is repeated. We regard this as geometric evidence of shear-induced chaos.

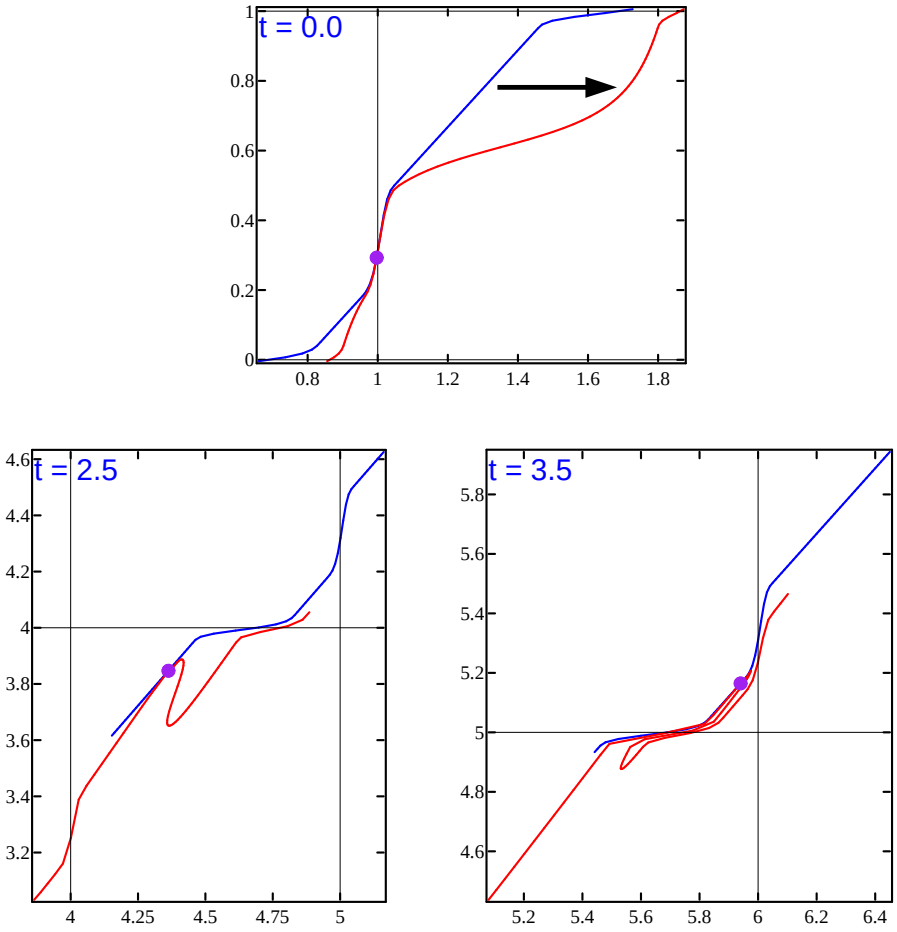

Figure 11: Snapshots of the limit cycle and its kicked image in a moving frame. *Blue curves:* Φ_t-images of γ_0, the part of the limit cycle between $\theta_2 = 0$ and $\theta_2 = 1$. *Red curves:* $\kappa(\gamma_0)$ and its images. *Purple dot:* the point on γ_0 which does not move under κ. The parameters are the same as in Fig. 10.

We have seen that in the phase-locked regime, the folding of the limit cycle (when the time interval between kicks is sufficiently large) can be deduced from the geometry of the strong stable foliation. A natural question is: in the quasi-periodic regime, are there geometric clues in the unforced dynamics that will tell us whether the system is predisposed to chaotic behavior when forced? Since folding occurs in finite time, we believe the answer lies partially in what we call *finite-time stable manifolds*, a picture of which is shown in Fig. 13. We first explain what these manifolds are before discussing what they can — and cannot — tell us.

Fix $t > 0$. At each $z \in \mathbb{T}^2$, let $V(z)$ be the most contracted direction of the linear map $D\Phi_t(z)$ if it is uniquely defined, *i.e.* if v is a unit tangent vector at z in the direction $V(z)$, then $|D\Phi_t(z)v| \leq |D\Phi_t(z)u|$ for all unit tangent vectors u at z. A smooth curve is called a *time-t stable manifold* if it is tangent to V at all points; these curves together form the *time-t stable foliation*. In general, time-t stable manifolds are not necessarily defined everywhere; they vary with t, and may not stabilize as t increases. When "real" (*i.e.* infinite-time) stable manifolds exist, time-t stable manifolds converge to them as $t \to \infty$.

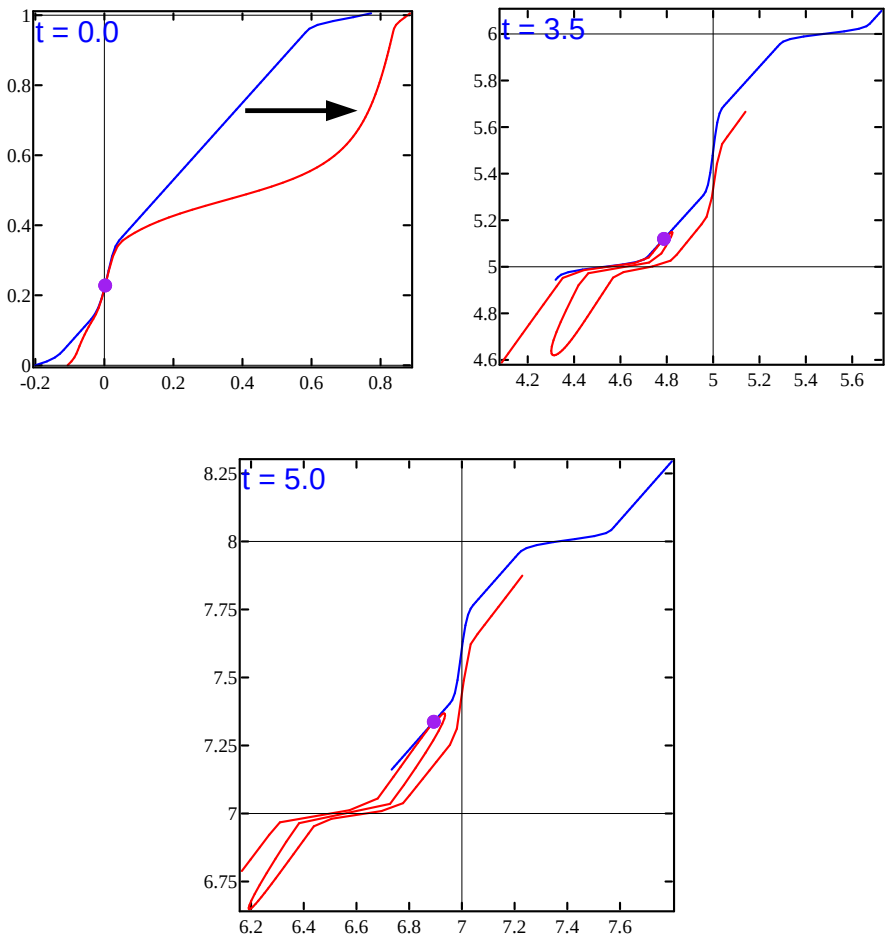

Figure 12: Snapshots of an orbit segment and its image after a single kick in a moving frame, for the system (10) in a near-periodic regime. *Blue curves:* a segment γ_0 of an orbit and its forward images $\Phi_t(\gamma_0)$ at $t = 3.5, 5$. *Red curves:* $\kappa(\gamma_0)$ and its forward images. *Purple dot:* the point on γ_0 which does not move under κ. The parameters are $\nu_1 = 1$, $\nu_2 = 1.1$, $a_{\text{ff}} = 1$, and $a_{\text{fb}} = 1.2$.

The blue curve in Fig. 13 is an orbit segment of Φ_t. The angles between this segment and the time-5 stable manifolds (*green curves*) reflect the presence of shear. For example, if a kick sends points on the blue curve to the right, then within 5 units of time most points on the kicked segment will lag behind their counterparts on the original orbit segment — except for the point with $\theta_1 = 0$ at the time of the kick. Pinching certain points on an orbit segment while having the rest slide back potentially creates a scenario akin to that in Fig. 2; see Sect. 1.2. One is also likely to find shear along the black curve in Fig. 13, a second orbit segment of Φ_t. Whether or not the shear here is strong enough to cause the formation of folds in 5 units of time cannot be determined from the foliation alone; more detailed information such as contraction rates are needed. What Fig. 13 tells us are the mechanism and the shapes of the folds if they *do* form. Notice also that shearing occurs in opposite directions along the blue and black segments. This brings us to a complication not present previously: each orbit of Φ_t spends only a finite amount of time near, say, the blue

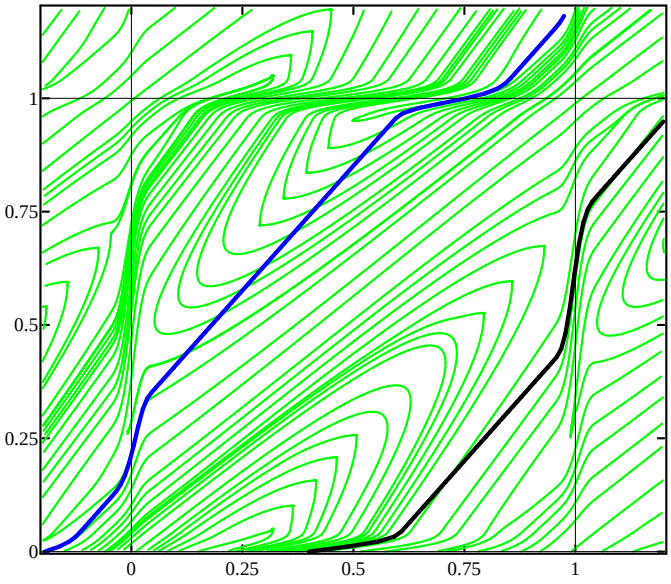

Figure 13: The time-5 stable foliation of the system (10) in a near-periodic regime. *Blue & black curves:* two orbit fragments. *Green curves:* time-5 stable foliation. The parameters here are the same as in Fig. 12.

curve before switching to the region near the black curve, and when it does so, it also switches the direction of shear. Finite-time stable foliations for system (10) have also been computed for $t \in \{3, 5\}$ and a sample of $a_{\text{fb}} \in (1.1, 1.6)$ (not shown). They are qualitatively similar to Fig. 13, with most of the leaves running in a northeasterly direction.

In summary, for t not too large, time-t stable foliations generally do not change quickly with t or with system parameters. They are good indicators of shear, but do not tell us if there is *enough* shear for folds to form. For the system defined by (10), given that the finite-time stable manifolds are nearly parallel to flowlines and the kick map acts unevenly with respect to this foliation, we conclude the presence of shear. Fig. 12 and similar figures for other a_{fb} (not shown) confirm that folding does indeed occur when the system is forced in the near-periodic regime.

Computation of Lyapunov exponents

To provide quantitative evidence of shear-induced chaos in the situations discussed above, we compute $\Lambda_{\max}$. Recall that while periodic kicks followed by long relaxations provide a simple setting to visualize folding, it is not expected to give clean results for $\Lambda_{\max}$ because of the competition between transient and sustained chaos (see Sect. 1.2). Continuous-time random forcing, on the other hand, produces numerical results that are much easier to interpret.

Study 4a: Stochastic Forcing. We consider system (10) with $a_{\text{ff}} = 1$ and $a_{\text{fb}} \in [1.1, 1.6]$. The forcing is of the form $I(t) = a \cdot dB_t$ where B_t is standard Brownian motion.

Study 4b: Periodic kicks. The equation and parameters are as above, and the forcing is given by $I(t) = A \cdot \sum_n \delta(t - nT)$.

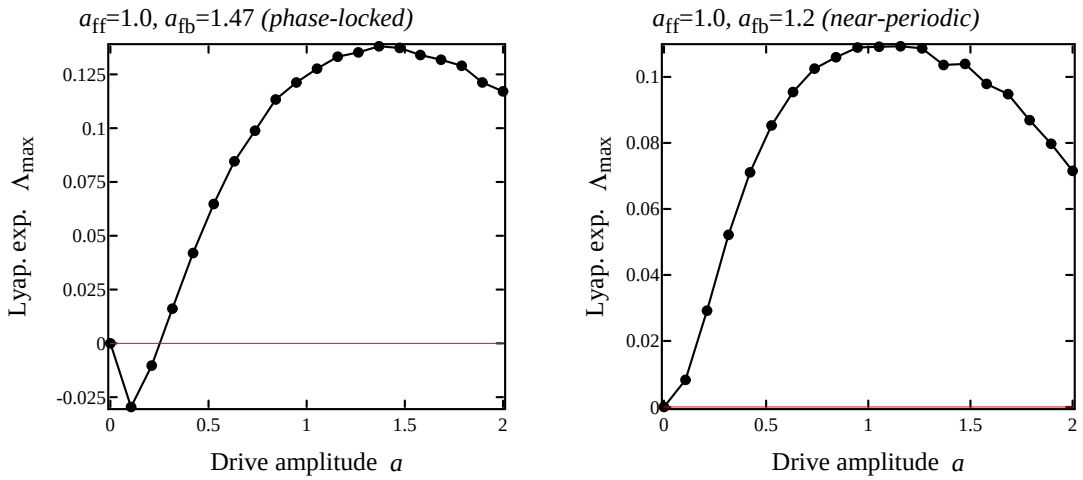

Figure 14: Lyapunov exponent of the system (10) subjected to white noise forcing. The parameters correspond to those in Figs. 10 and 12, respectively.

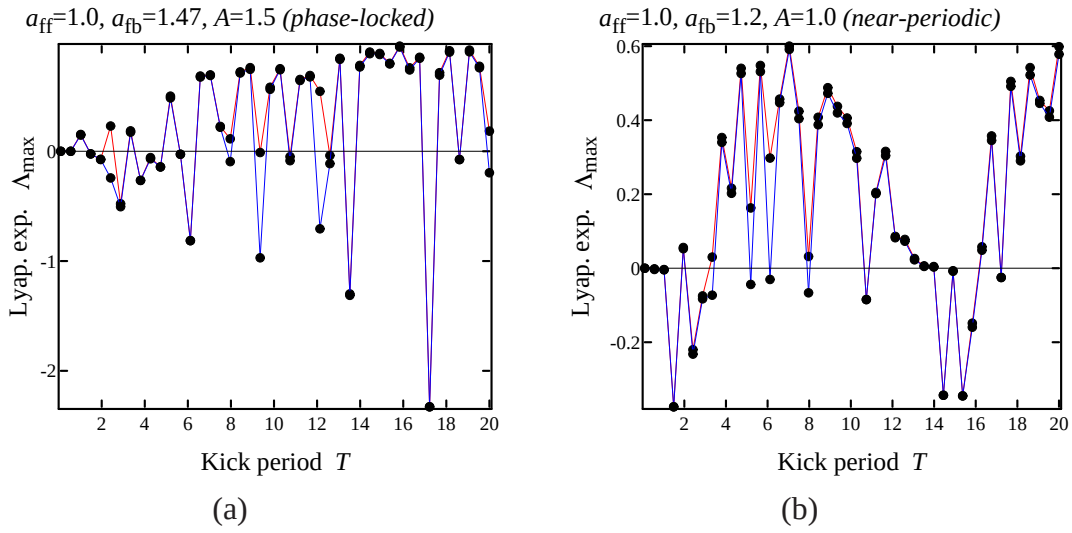

Figure 15: Lyapunov exponent of the system (10) subjected to periodic kicks. The parameters correspond to those in Figs. 10 and 12, respectively. As in Study 1, we show both upper and lower estimates of $\Lambda_{\max}$.

Summary of Findings. *Positive $\Lambda_{\max}$ are found for stochastic forcing in the parameter interval studied, both before and after the onset of phase-locking at $a_{\rm fb} = a^*_{\rm fb}$. For periodic kicks with large enough A and T, it appears that $\Lambda_{\max}$ is positive for a fraction of the forcing periods tested, but the results are hard to interpret due to the competition between transient and sustained chaos.*

Supporting Numerical Evidence. Fig. 14 shows some results for stochastic forcing. For $a_{\rm fb} = 1.47$, negative Lyapunov exponents are found for very small amplitudes of forcing, while slightly stronger forcing (*e.g.* $a \approx 0.4$) is needed before $\Lambda_{\max} > 0$ can be concluded with confidence. In contrast, even fairly small values of forcing seem to lead to $\Lambda_{\max} > 0$ when $a_{\rm fb} = 1.2$, *i.e.* in the

near-periodic regime. This may be explained by the damping in the limit cycle case, especially for larger $a_{\rm fb}$. Notice also that in this model large amplitudes of forcing do not lead to larger $\Lambda_{\max}$. This is due to the fact that unlike the system in Studies 1–3, a very strong forcing merely presses most of the phase space against the circle $\theta_1 = 0$, which is not very productive from the point of view of folding phase space. Fig. 15 shows plots of $\Lambda_{\max}$ for periodic kicks. Here, roughly 40% of the kick periods T for which Lyapunov exponents were computed yield a positive exponent. More generally, we find that $\Lambda_{\max} > 0$ for over 40% of kick intervals T as A varies over the range $[0.75, 1.5]$. See Simulation Details in Study 1.

Conclusions

Shear-induced chaos, by which we refer to the phenomenon of an external force interacting with the shearing in a system to produce stretches and folds, is found to occur for wide ranges of parameters in forced oscillators and quasi-periodic systems. Highlights of our results include:

(i) For periodically kicked oscillators, positive Lyapunov exponents are observed under quite modest impositions on the unforced system and on the relaxation time between kicks (in contrast to existing rigorous results). These regimes are, as expected, interspersed with those of transient chaos in parameter space.

(ii) Continuous-time stochastic forcing is shown to be equally effective in producing chaos. The qualitative dependence on parameters is similar to that in deterministic forcing. We find that suitably directed, degenerate white noise is considerably more effective than isotropic white noise (and additive noise will not work). We have also found evidence for an approximate scaling law relating $\Lambda_{\max}$ to σ, λ, and a. Other types of random forcing such as Poisson kicks are also studied and found to produce chaos.

(iii) The shear-induced stretching-and-folding mechanism can operate as well in quasi-periodic systems as it does in periodic systems, *i.e.* limit cycles are not a precondition for shear-induced chaos. We demonstrate this through a pulse-coupled 2-oscillator system. Chaos is induced under both periodic and white noise forcing, and a geometric explanation in terms of finite-time stable manifolds is proposed.

The conclusions in (i) and (ii) above are based on systematic numerical studies of a linear shear flow model. As this model captures the essential features of typical oscillators, we expect that our conclusions are valid for a wide range of other models. Our numerical results, particularly those on stochastic forcing, point clearly to the possibility of a number of (rigorous) theorems.

References

[1] L. Arnold, *Random Dynamical Systems*, Springer-Verlag (1998)

[2] L. Arnold, N. Sri Namachchivaya, K. R. Schenk-Hoppé, "Toward an understanding of stochastic Hopf bifurcation: a case study," *Int. J. Bifur. and Chaos* **6** (1996) *pp.* 1947–1975

[3] E. I. Auslender and G. N. Mil'shteĭn, "Asymptotic expansions of the Liapunov index for linear stochastic systems with small noise," *J. Appl. Math. Mech.* **46** (1982) *pp. 358–365*

[4] P. H. Baxendale, "A stochastic Hopf bifurcation," *Probab. Theory and Related Fields* (1994) *pp.* 581–616

[5] P. H. Baxendale, "Lyapunov exponents and stability for the stochastic Duffing-van der Pol oscillator," *IUTAM Symposium on Nonlinear Stochastic Dynamics*, Kluwer (2003) *pp.* 125–135

[6] P. H. Baxendale, "Stochastic averaging and asymptotic behavior of the stochastic Duffing-van der Pol equation," *Stochastic Process. Appl.* **113** (2004) *pp.* 235–272

[7] P. H. Baxendale, "Lyapunov exponents and resonance for small periodic and random perturbations of a conservative linear system," *Stoch. Dyn.* **2** (2002) *pp.* 49–66

[8] P. H. Baxendale and L. Goukasian, "Lyapunov exponents for small random perturbations of Hamiltonian systems," *Annals of Probability* **30** (2002) *pp.* 101–134

[9] J. Guckenheimer, "Isochrons and phaseless sets," *J. Theor. Biol.* **1** (1974) *pp.* 259–273

[10] J. Guckenheimer and P. Holmes, *Nonlinear Oscillations, Dynamical Systems, and Bifurcations of Vector Fields*, Springer-Verlag (1983)

[11] J. Guckenheimer, M. Weschelberger, and L.-S. Young, "Chaotic attractors of relaxation oscillators," *Nonlinearity* **19** (2006) *pp.* 701–720

[12] Yu. Kifer, *Ergodic Theory of Random Transformations*, Birkhäuser (1986)

[13] H. Kunita, *Stochastic Flows and Stochastic Differential Equations*, Cambridge University Press (1990)

[14] K. K. Lin, E. Shea-Brown, L.-S. Young, "Reliable and unreliable dynamics in driven coupled oscillators," preprint (2006); arXiv:nlin/0608021v1

[15] K. K. Lin, E. Shea-Brown, L.-S. Young, "Reliable and unreliable dynamics in coupled oscillator networks," in preparation

[16] N. Sri Namachchivaya, "The asymptotic stability of a weakly perturbed 2-dimensional non-Hamiltonian system", private communication

[17] A. Oksasoglu and Q. Wang, "Strange attractors in periodically-kicked Chua's circuit," *Int. J. Bifur. Chaos* **16** (2005) *pp.* 83–98

[18] M. Pinsky and V. Wihstutz, "Lyapunov exponents of nilpotent Itô systems," *Stochastics* **25** (1998) *pp.* 43–57

[19] K. R. Schenk-Hoppé, "Bifurcation scenarios of the noisy Duffing-van der Pol oscillator," *Nonlinear Dynamics* **11** (1996) *pp.* 255–274

[20] D. Taylor and P. Holmes, "Simple models for excitable and oscillatory neural networks," *J. Math. Biol.* **37** (1998) *pp.* 419–446

[21] B. van der Pol and J. van der Mark, "Frequency demultiplication,"*Nature* **120** (1927) *pp.* 363–364

[22] Q. Wang and L.-S. Young, "Strange attractors with one direction of instability," *Comm. Math. Phys.* **218** (2001) *pp.* 1–97

[23] Q. Wang and L.-S. Young, "From invariant curves to strange attractors," *Comm. Math. Phys.* **225** (2002) *pp.* 275–304

[24] Q. Wang and L.-S. Young, "Strange attractors in periodically-kicked limit cycles and Hopf bifurcations," *Comm. Math. Phys.* **240** (2003) *pp.* 509–529

[25] Q. Wang and L.-S. Young, "Toward a theory of rank one attractors," *Annals of Mathematics* (to appear)

[26] A. Winfree, *The Geometry of Biological Time, Second Edition*, Springer-Verlag (2000)

[27] G. Zaslavsky, "The simplest case of a strange attractor," *Physics Letters* **69A** (1978) *pp.* 145–147